ACBD2/ECI2-Mediated Peroxisome-Mitochondria Interactions in Leydig Cell Steroid Biosynthesis

Jinjiang Fan, Xinlu Li, Leeyah Issop, Martine Culty, and Vassilios Papadopoulos

The Research Institute of the McGill University Health Centre (J.F., X.L., L.I., M.C., V.P.) and Departments of Medicine (J.F., L.I., M.C., V.P.), Biochemistry (X.L., V.P.), and Pharmacology and Therapeutics (M.C., V.P.), McGill University, Montréal, Québec, Canada H4A 3J1

Fatty acid metabolism and steroid biosynthesis are 2 major pathways shared by peroxisomes and mitochondria. Both organelles are in close apposition to the endoplasmic reticulum, with which they communicate via interorganelle membrane contact sites to promote cellular signaling and the exchange of ions and lipids. To date, no convincing evidence of the direct contact between peroxisomes and mitochondria was reported in mammalian cells. Hormone-induced, tightly controlled steroid hormone biosynthesis requires interorganelle interactions. Using immunofluorescent staining and live-cell imaging, we found that dibutyryl-cAMP treatment of MA-10 mouse tumor Leydig cells rapidly induces peroxisomes to approach mitochondria and form peroxisome-mitochondrial contact sites/fusion, revealed by the subcellular distribution of the endogenous acyl-coenzyme A-binding domain (ACBD)2/ECI2 isoform A generated by alternative splicing, and further validated using a proximity ligation assay. This event occurs likely via a peroxisome-like structure, which is mediated by peroxisomal and mitochondrial matrix protein import complexes: peroxisomal import receptor peroxisomal biogenesis factor 5 (PEX5), and the mitochondrial import receptor subunit translocase of outer mitochondrial membrane 20 homolog (yeast) protein. Similar results were obtained using the mLTC-1 mouse tumor Leydig cells. Ectopic expression of the ACBD2/ECI2 isoform A in MA-10 cells led to increased basal and hormone-stimulated steroid formation, indicating that ACBD2/ECI2-mediated peroxisomes-mitochondria interactions favor in the exchange of metabolites and/or macromolecules between these 2 organelles in support of steroid biosynthesis. Considering the widespread occurrence of the ACBD2/ECI2 protein, we propose that this protein might serve as a tool to assist in understanding the contact between peroxisomes and mitochondria. (*Molecular Endocrinology* 30: 763–782, 2016)

Peroxisomes and mitochondria have been closely related in terms of their synergetic functioning in the metabolism of fatty acids and reactive oxygen species, as well as in steroid biosynthesis (1–3). Both organelles make contact with the endoplasmic reticulum (ER) via interorganelle membrane contact sites. These interactions with the ER support cellular signaling and ion/lipid exchanges (4), as well as organelle biogenesis, where the ER assists the mitochondria in defining the position of mitochondrial division sites (5–7), and where it can also provide a base for the origin of peroxisomes (8–10). One-way communication from mitochondria to peroxisomes has been proposed to occur via mitochondria-derived vesicles, but no convincing evidence exists supporting the direct contact between peroxisomes and mitochondria in mammalian cells, even though there are a few reports from unicellular yeasts (11–13). However, whether these subcellular systems between yeasts and mammals are comparable is widely controversial (14, 15).

ISSN Print 0888-8809 ISSN Online 1944-9917
Printed in USA

Received January 13, 2016. Accepted May 4, 2016.
First Published Online May 11, 2016

Abbreviations: ACBD, acyl-CoA-binding domain; ACBP, acyl-CoA-binding protein domain; CoA, coenzyme A; COX IV, cytochrome c oxidase subunit 4; dbcAMP, dibutyryl-cAMP; DAPI, 4′,6-diamidino-2-phenylindole; ECH, enoyl-CoA hydratase; ECI2, enoyl-CoA-δ isomerase 2; ER, endoplasmic reticulum; FBS, fetal bovine serum; GAPDH, glyceraldehyde-3-phosphate dehydrogenase; GSEA, gene set enrichment analysis; In-cell co-IP, in-cell coimmunoprecipitation; H+L, Heavy + Light chains; OMM, outer mitochondrial membrane; P*, peroxisomal cargo; PECI, peroxisomal Δ3,Δ2-enoyl-CoA isomerase; PEX5, peroxisomal biogenesis factor 5; -PKL, a peroxisomal targeting signal 1 tripeptide -proline-lysine-leucine; PLA, proximity ligation assay; PMP70, the 70-kDa peroxisomal membrane protein; PTS1, peroxisomal targeting signal-1; qRT-PCR, quantitative real-time PCR; Rr, Pearson's correlation coefficient; SCP, sterol carrier protein; siRNA, Small interfering RNA; TOMM20, translocase of OMM 20 homolog (yeast) protein; VDAC1, voltage-dependent anion-selective channel protein 1.

Peroxisomes and mitochondria share several components in steroid biosynthesis as well as in fatty acid metabolism (16–18). A family of acyl-CoA-binding domain (ACBD)-containing proteins is strongly linked to this process, where the ACBD3/PAP7 and ACBD1/DBI play significant roles in steroidogenesis (19, 20). However, less information is available regarding the ACBD2 or enoyl-CoA-δ isomerase 2 (ECI2) member of the family. It is of great interest that ACBD2/ECI2 has been reported to be a peroxisomal and/or mitochondrial protein, implying that it plays a role in both organelles. ACBD2/ECI2 has been confusingly named as either mitochondrial ECI2 or peroxisomal Δ3,Δ2-enoyl-CoA isomerase (PECI) (21). Due to its dual subcellular localization, determined by Nycodenz gradient centrifugation, PECI was renamed ECI (22), even though ECI is actually a general term to describe enzymes that convert *cis*- or *trans*-double bonds of fatty acids at γ-carbon to transdouble bonds at β-carbon. The circumstances under which the ACBD2/ECI2 protein targets either peroxisomes and/or mitochondria remain unclear, thus hampering investigations of the cellular functions of this protein. Both its core domains, ECI/enoyl-CoA hydratase (ECH) and ACBD, are relevant to fatty acid metabolism. ACBD2/ECI2 has a similar function as ECI1 in the metabolism of unsaturated fatty acids, as *Eci1* knockout mice show no pronounced phenotype, but knockdown of *Eci2* in *Eci1*-deficient fibroblasts show an accumulation of C12:1 acylcarnitine (23, 24). As a matter of fact, the existence of a third paralogous gene, *Eci3*, with high sequence similarity to *Eci2*, makes the story intriguing. Furthermore, *Acbd2/Eci2* has 3 known sequence varieties that are generated from alternative pre-mRNA splicing events, which are one of the mechanisms involved in the posttranscriptional regulation of gene expression, leading to a wide variety of gene products (25). The biological significance of alternative splicing events of the *Acbd2/Eci2* gene, however, remains unknown.

In the testis, peroxisomes were initially thought to be exclusively present in the interstitial Leydig cells where the androgen testosterone important for the establishment of the male sexual characteristics and fertility is produced (26). Steroid hormone biosynthesis is the result of multiple biological processes, with the rate-limiting step involving the import of the substrate cholesterol, originating from various intracellular sources, into mitochondria, a process mediated by a protein complex in the outer mitochondrial membrane (OMM) (27–30). In rat Leydig cells, equivalent amounts of free and esterified cholesterol are present before and after hormone stimulation (31). During steroidogenesis, the remaining side-product free acyl moieties cholesterol esters must be shuttled into either the mitochondria and/or the peroxisomes for β-oxidation, resulting in the production of ATP and/or the formation of hydrogen peroxide. Peroxisomes present in Sertoli and germ cells have low level of catalase, which is different from that found in Leydig cells (32–34). The low levels of catalase, a peroxisomal marker, in Sertoli and germ cell peroxisomes suggest that multiple forms of peroxisomes exist; these forms are characterized by distinct morphology and/or different composition of their matrix proteins (35).

We demonstrate here, for the first time, that the subcellular distribution of ACBD2/ECI2 revealed a molecular basis of the close contact/fusion between peroxisomes and mitochondria occurring via a "peroxisome-like structure" loaded with C-terminal peroxisomal targeting signal-1 (PTS1) peroxisomal matrix proteins. The proximity between the peroxisomal ACBD2/ECI2 and mitochondrial import receptor subunit translocase of OMM 20 homolog (yeast) protein (TOMM20) was validated using in-cell coimmunoprecipitation (In-cell co-IP) methodology. This process involves 2 organelle matrix protein import receptor complexes: PEX5 and TOMM20, which can be visualized by the dual targeting of ACBD2/ECI2 with a fluorescent tag. Subcellular distribution of ACBD2/ECI2 isoform A has mechanistic implications in peroxisome-mitochondria contact and in the support of steroid biosynthesis.

Materials and Methods

Sequence analysis and microarray data procession

Protein domain structures were retrieved from Pfam 27.0 (http://pfam.sanger.ac.uk). Each nucleotide sequence and its corresponding deduced peptide sequence of proteins was retrieved from GenBank (http://www.ncbi.nlm.nih.gov/genbank) using mouse ACBD2/ECI2 sequence as a query. The top 500 sequences with a hit were used for further sequence analysis. Sequence alignments were performed using ClustalW (36), and phylogenetic trees were constructed in MEGA5 using the neighbor-joining method, with the optional setting of Dayhoff PAM matrices and pairwise deletion (37, 38). The data from the Affymetrix arrays were analyzed using FlexArray Software V1.6 (Genome Quebec Innovation Center; http://gqinnovationcenter.com). Raw probe intensity data in the Affymetrix CEL files were evaluated first, with noisy scanning datasets removed from further analysis. The raw gene expression data were normalized using the robust multichip average algorithm (39). The comparison of datasets was performed using ANOVA within the FlexArray Software V1.5 to test for differences across the experimental factors (time points, replicates, and individual genes). Genes with significant changes during cellular differentiation, which were identified with a cut-off $P = .001$, were further analyzed by fold changes. Gene set enrichment analysis (GSEA) was performed; statistically significant, concordant differences in a set of genes, as defined from the Molecular Signature Database, were evaluated using the GSEA (www.broad.mit.edu/gsea/)

(40). A false discovery rate for each set of genes was estimated on the probability that a gene set with a given new enrichment score represents a false-positive finding. The nominal *P* value was estimated to show the statistical significance of the enrichment score for a single gene set.

cDNAs, cloning, antibodies, subcellular fractioning, and immunoblotting

Expressed sequence tag clones of mouse *Acbd2/Eci2*, *Eci1*, *Eci3*, *Tomm20*, *Pmp70(Abcd3)*, and *Pex11β* cDNAs were selected for their possession of the longest inserts from Open Biosystems (http://dharmacon.gelifesciences.com). To make a fusion protein with Discosoma red fluorescent protein monomer (DsRed) tag, the open reading frame of each gene was subcloned into either pDsRed-Monomer-N1 or pDsRed-Monomer-C1 (Clontech) vector: pAcbd2/Eci2-DsRed, pEci1-DsRed, pEci3-DsRed, pDsRed-Acbd2/Eci2, pDsRed-Eci1, and pDsRed-Eci3. Plasmid mito-DsRed-Eci2 derived from pDsRed-Acbd2/Eci2 was constructed by moving the presequence of ACBD2/ECI2 to the front of DsRed. To visualize organelle juxtaposition, the plasmid mito-DsRed-pero derived from pmito-DsRed-Eci2 was constructed via replacement of the *Acbd2/Eci2* gene by a peroxisomal sequence tripeptide -proline-lysine-leucine (−PKL). In a similar strategy, to make a blue fluorescent fusion protein (AmCyan) targeting peroxisomes, we made pAmCyan-pero. The pmito-BFP (mitochondria in blue) was purchased from Addgene. Both plasmids (pAmCyan-mPEX11β and plasmid mouse 70-kDa peroxisomal membrane protein (PMP70)) are fused with AmCyan tag using the pAmCyan-C1 vector. The pm-TOMM20 was made fused with the cyan fluorescent protein tag using the pCFP-N1 vector (Clontech). The plasmid mito-roGFP1 with the mitochondrial targeting sequence in pEGFP-N1 for mammalian expression (pRA306) was a gift from James Remington at the University of Oregon. Oligos from all plasmid constructs are listed in Supplemental Table 1. For immunostaining, we used the primary goat anti-PECI polyclonal antibody (P-19; sc-82692; Santa Cruz Biotechnology, Inc) and the secondary Alexa Fluor 488 donkey antigoat IgG Heavy + Light chains (H+L) antibody (A-11055; Molecular Probes) (Table 1).

As to the subcellular fractioning, MA-10 mouse tumor Leydig cells (gift from Dr Mario Ascoli, University of Iowa) were grown in 150-mm dishes to 70% confluence, washed with PBS, and then harvested for further process. In brief, to prepare crude membranes, cells were homogenized with a glass potter followed by 3 cycles of freezing and thawing in isolation buffer 1 (225mM mannitol, 75mM sucrose, and 30mM Tris-HCl; pH 7.4). Homogenates were centrifuged at 800*g* for 5 minutes at 4°C. The collected supernatants (containing cytosolic proteins) were centrifuged twice 11 000*g* for 10 minutes at 4°C to obtain crude mitochondria. These preparations were resuspended in isolation buffer 2 (250mM mannitol, 5mM HEPES [pH 7.4], and 0.5mM EGTA). To confirm the enrichment of the crude mitochondrial fraction, we performed immunoblots analysis using rabbit polyclonal anticytochrome c oxidase subunit 4 (COX IV) antibody (ab16056; Abcam) as mitochondrial loading control, rabbit monoclonal antisterol carrier protein (SCP)2 antibody (EPR9022), 58 kDa (ab140126; Abcam), as peroxisome marker, rabbit polyclonal antiglyceraldehyde-3-phosphate dehydrogenase (GAPDH) antibody (2275-PC-100; Trevigen) as whole protein loading control, and finally mouse monoclonal anti-ACBD2/ECI2 (sc-136374; PECI Antibody) as the target protein detection (Table 1).

Establishment of the homogeneous stable cell line Mito-H by fluorescence-activated cell sorting

Mouse MA-10 Leydig tumor cells were used to establish the stable expression of mitochondrial roGFP1 (41, 42). Briefly, MA-10 cells transfected with 4-μg plasmid pRA306 were grown in DMEM/F-12 medium supplemented with 5% heat-inactivated fetal bovine serum (FBS) and 2.5% horse serum at 37°C and 5% CO_2. Cells were initially supplemented with 500 μg/mL of G418 and then maintained in the same medium with 400 μg/mL of G418. The stable expansion of a single colony was further sorted by using a BD FACSAria II (high-speed cell sorter) to separate cells with high expression of roGFP, desig-

Table 1. Information About the Antibodies Used

Peptide/Protein Target	Antigen Sequence (if Known)	Name of Antibody	Manufacturer, Catalog Number, or Name of Source	Species Raised in Monoclonal or Polyclonal	Dilution Used (IF, IB)
PECI/ECI2/ACBD2		Anti-PECI	Santa Cruz Biotechnology, Inc, P-19; sc-82692	Goat	1:100 (IF)
TOMM20		Anti-TOM20	Santa Cruz Biotechnology, Inc, FL-145; sc-11415	Rabbit	1:100 (IF)
PECI/ECI2/ACBD2		Anti-PECI	Santa Cruz Biotechnology, Inc, 32; sc-136374	Mouse	1:100 (IF); 1:1300
VDAC1		Anti-VDAC1	Santa Cruz Biotechnology, Inc, B6; sc-390996	Mouse	1:1300
COX IV		Anti-COX IV	Abcam, ab16056	Rabbit	1:1300
SCPX		Anti-SCP2	Abcam, ab140126	Rabbit	1:1000
GAPDH		Anti-GAPDH	Trevigen, 2275-PC-100	Rabbit	1:5000
Rabbit IgG		HRP-linked antibody	Cell Signaling Technology, 7074	Goat	1:1300
Mouse IgG		HRP-linked antibody	Cell Signaling Technology, 7076	Horse	1:1300
Biotin		HRP-linked antibody	Cell Signaling Technology, 7075	Goat	1:3000
Rabbit IgG		Rabbit IgG (H + L)	Molecular Probes, A10040	Donkey	1:500
Mouse IgG		Antimouse IgG (H + L)	Molecular Probes, P31582	Goat	1:500
Goat IgG		Antigoat IgG (H + L)	Molecular Probes, A-11055	Donkey	1:500

nated as Mito-H (124 128 cells), and cells with a low expression of roGFP, designated as Mito-L (144 610 cells). Cells were grown in the same medium but with the addition of 1% penicillin/streptomycin for 2 passages. After cell splitting, Mito-H cells were maintained in DMEM/F-12 medium containing 400 μg/mL of G418.

Cell culture, plasmid transfection, small interfering RNA (siRNA) knockdown, confocal laser microscopy live imaging, and immunofluorescence microscopy

Mito-H cells were maintained in DMEM/F-12 medium supplemented with 5% heat-inactivated FBS, 2.5% horse serum, and 400 μg/mL of G418. MA-10 cells were incubated under the same conditions, except without adding G418. mLTC1 mouse tumor Leydig cells were obtained from ATCC and cultured in RPMI 1640 medium containing 10% FBS, according to the guidelines provided by the supplier. Knockdown of the *Pex5* gene in MA-10 cells was performed using Peroxin 5 siRNA (m) (Santa Cruz Biotechnology, Inc), and the knockdown of *Acbd2/Eci2* gene was carried out using PECI siRNA (m) (Santa Cruz Biotechnology, Inc). The control siRNA (Santa Cruz Biotechnology, Inc) was used as negative control(s). For confocal laser microscopy live imaging, cells were cultured in 35 mm Fluoro-Dish sterile culture dishes (World Precision Instruments) to 75% confluence. The next day, cells were transfected with plasmids of interest using Lipofectamine 2000 (Invitrogen). At 24 hours after transfection, cells were incubated with Hoechst 33342 (Invitrogen) to counterstain nuclear DNA. Cells were examined using a scanning laser confocal microscope (Olympus FluoView FV1000) with an oil immersion objective (UPLSAP, $\times$100) and the following excitation/emission wavelengths (nm): blue (Hoechst) 350/461, green (roGFP) 498/516, and red (DsRed) 558/583. Images from a single optical slice were captured with FluoView software (version 3.1; Olympus), and a representative single optical slice of each image was presented, after processed using Image-Pro Plus (version 6.3). Pearson's correlation coefficient (Rr) for fluorescent images was calculated using the intensity correlation analysis, a plugin for ImageJ (http://imagej.nih.gov). Statistical analysis of quantitative data was performed using Student's *t* tests and Mann-Whitney tests (Prism V.5.0).

For the immunofluorescence microscopy, the MA-10 cells cultured overnight with 50% confluence were treated with 1mM dibutyryl-cAMP (dbcAMP) for 2 hours and then stained with MitoTracker CMXRos (Invitrogen) for 20 minutes at 37°C. The cells were fixed in a 4% paraformaldehyde solution plus 0.1% Triton X-100 in PBS for 5 minutes and washed in PBS for 5 minutes. After blocking with 1% BSA in PBS plus 10% donkey normal serum for 30 minutes at 37°C, the cells were incubated with goat anti-PECI polyclonal antibody (Santa Cruz Biotechnology, Inc) overnight. The secondary antibody, Alexa Fluor 488 donkey antigoat IgG (H+L) antibody (Invitrogen), was applied to the cells for 1 hour at room temperature (Table 1). Cells were mounted using UltraCruz mounting medium containing 4′,6-diamidino-2-phenylindole (DAPI) (Santa Cruz Biotechnology, Inc).

Proximity ligation assay (PLA) or Duolink-In-cell co-IP

The interaction between the peroxisomal protein ACBD2/ECI2 and the OMM marker TOMM20 was detected by in situ PLA, the Duolink in situ orange starter kit goat/rabbit kit (DUO92106, O-Link; Bioscience). The PLA probe antirabbit minus binds to the TOMM20 antibody (Santa Cruz Biotechnology, Inc), whereas the PLA probe antigoat plus binds to the PECI antibody (Table 1). The procedure followed was as recommended by the manufacturer. In brief, a signal with Duolink PLA is generated if ACBD2/ECI2 and TOMM20 proteins are within 40-nm proximity (43). After preincubation with a blocking buffer (1% BSA in 1$\times$ PBS or plus 10% goat normal serum) for 1 hour, MA-10 cells or mLTC1 cells treated with or without dbcAMP submitted to 4% PFA fixation and 0.1% fresh Triton X-100 permeabilization were incubated overnight with the primary antibodies to PECI (1:150) and TOM20 (1:100). All wash steps were performed using 1$\times$ PBS. Images were acquired using the Olympus FLUOVIEW FV1000 confocal laser scanning microscope, processed using FluoView software (version 3.1; Olympus) and digitally quantified using Duolink ImageTool (Olink Bioscience). The bar graph of the blob numbers reflecting the PLA signals and statistical analysis were performed using GraphPad Prism version 5.00 (GraphPad).

Steroid measurement by RIA

RIA was performed, as previously described (44, 45). Briefly, cells were plated at 0.3×10^6 cells per well into 6-well plates overnight, washed with serum-free medium, and left untreated or treated for 2 hours with 1mM dbcAMP. Culture media were collected, and progesterone production was measured by RIA using antiprogesterone antisera (MP Biomedicals) and [1,2,6,7-^{3}H] progesterone (specific activity 94.1 Ci/mmol; PerkinElmer Life Sciences) following the conditions recommended by the manufacturer. The intra- and interassay coefficients of variation were 2.6%–8.6% and 5.6%, respectively. Antiprogesterone antiserum was used at 1:1000 dilution after renaturation of the powder, as supplied by the provider. Progesterone production was normalized to the amount of protein in each well. RIA data were analyzed using Prism V. 5.0.

Quantitative real-time PCR (qRT-PCR), melting curve analysis, and sequencing

Total RNA at different time points from dbcAMP treatment was prepared with TRIzol reagent (Invitrogen) and then subject to deoxyribonuclease treatment and a removal reagent (DNA free; Ambion) before cDNA synthesis. RNA was subsequently diluted to 100 ng/μL using deoxyribonuclease/ribonuclease-free water, and first-strand cDNA was synthesized using the SuperScript first-strand synthesis system for qRT-PCR using the manufacturer's protocol (Invitrogen). The isoform-specific oligos listed in Supplemental Table 1 were used for qRT-PCR performed with the LightCycler 480 System (Roche Applied Science) in 20-μL reactions using 96-well microwell plates. Reaction mixtures, which included 2 μL of a 1:5 dilution of first-strand cDNA, 10 μL of LightCycler 480 SYBR Green 1 Master (Roche Applied Science), and each primer at a final concentration of 250nM, were added to each microwell. Reactions were cycled at 95°C for 5 minutes, followed by 45 cycles of 95°C for 10 seconds, 60°C for 10 seconds, and 72°C for 10 seconds, with a ramp rate of 4.4°C per

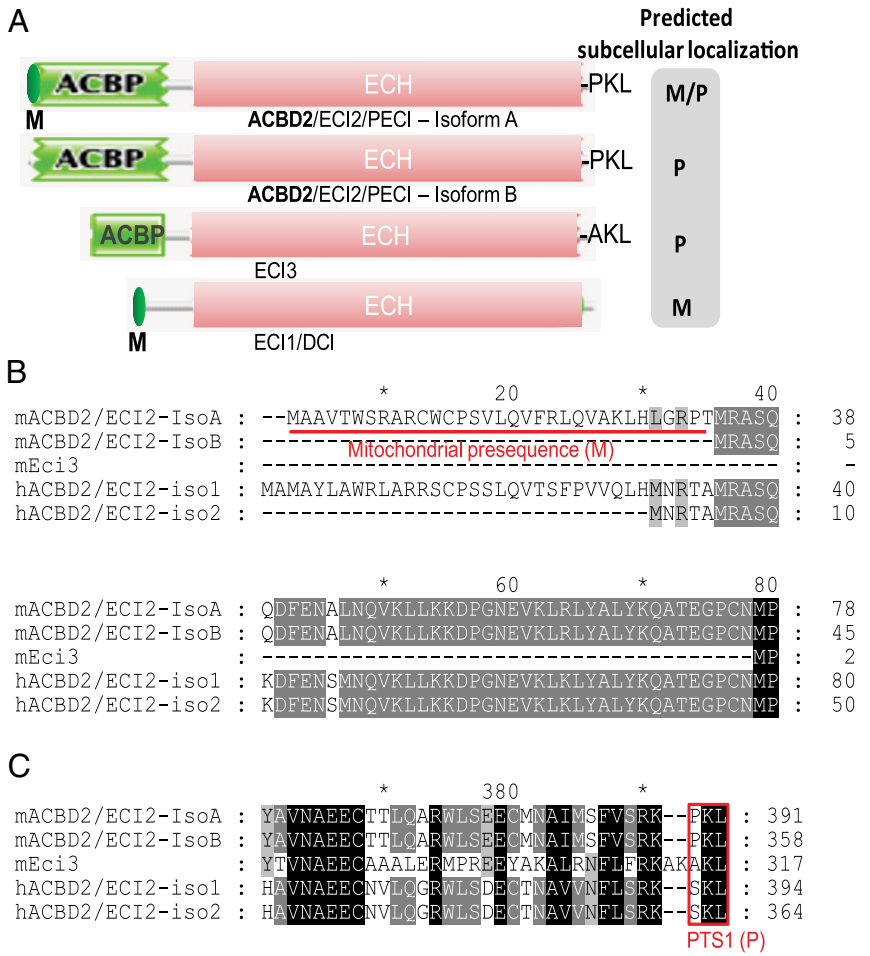

Figure 1. Domain structures, isoforms, and sequence alignments of ACBD2/ECI2 proteins and their closely related proteins. A, Comparison of the domain structures of ACBD2/ECI2, ECI3, and ECI1/DCI proteins. Potential mitochondrial targeting sequence or presequence (M) and putative PTS1s (P) are shown; the P sequences are indicated as −PKL (−Pro-Lys-Leu-COOH) and −AKL (−Ala-Lys-Leu-COOH). ECH catalyzes the hydration of 2-transenoyl-CoA into 3-hydroxyacyl-CoA. DCI, dodecenoyl-CoA isomerase as an alias for ECI1. B, Sequence alignment of the N termini of ACBD2/ECI2 isoforms and ECI3 proteins from mouse (m) and human (h). The putative mitochondrial presequences (M) are indicated for both human and mouse ACBD2/ECI2 isoform A (mACBD2/ECI2-IsoA and hACBD2/ECI2-Iso1). C, Sequence alignment of the C termini of ACBD2/ECI2 isoforms and ECI3 proteins as shown in B. The PTS1 (P) is indicated with a red box.

second, 2.2°C per second, and 4.4°C per second, respectively. Melting curve analysis was performed by 1 cycle of 95°C for 5 seconds, 65°C for 1 minute, 97°C for 0 seconds, and then 1 cycle of cooling at 40°C for 30 seconds. Results were analyzed using LightCycler 480 software (release 1.5.9; Roche Applied Science). Final PCR amplicons were also cloned into the pGEM-T easy vector (Promega) for sequencing at McGill University and the Genome Quebec Innovation Centre.

Results

ACBD2/ECI2 protein identity, molecular evolution, and functional gene expression profiling

ACBD2/ECI2 belongs to the ECI protein family, where all the members share a functional conserved ECI/ECH domain, but the ACBD2/ECI2 protein has an N-terminal acyl-CoA-binding protein domain (ACBP) domain and ECI3 possesses a partial ACBD domain (Figure 1A). The presence of both ACBP and ECH domains in one protein have led to the assigning of different names, such as ACBD2 or ECI2 or PECI (as peroxisomal ECI), respectively (20, 21). The ACBD2/ECI2 has been recorded as 2 protein isoforms, A and B, which are encoded by 3 recorded mRNA transcript varieties. In the ECI protein family, ECI3 and ECI1 (known as dodecenoyl-CoA isomerase) in the mouse genome are closely related to ACBD2/ECI2 (Figure 1A). Among the 4 proteins, both ACBD2/ECI2 isoform A and ECI1 have an N-terminal mitochondrial target sequence (M; presequence), whereas all 3 proteins (except ECI1) possess a C-terminal PTS1 sequence: −PKL or one conservative variant (P to the alanine, A): −AKL (Figure 1A). Deduced amino acid sequence alignments from both the N and C termini of mouse and human ACBD2/ECI2, as well as of ECI3, indicate that the ACBD2/ECI2 protein isoform A possesses a conserved presequence, but the rest have a PTS1 sequence at their C terminus, which falls within the generic PTS1 pattern in the eukaryotic linear motif resource for all eukaryotes: [SAPTC][KRH][LMFI]$ (http://elm.eu.org/elms/elmPages/TRG_PTS1.html) (Figure 1, B and C). The biological significance of the ACBD2/ECI2 isoform A with dual targeting properties has not yet been explored.

Because there is functional redundancy between ECI2 and ECI1 in unsaturated fatty acid oxidation, it is necessary to present a comprehensible view of this protein and its functional relationship to other members of ECI proteins. We systematically analyzed the phylogeny of ECI and other related gene families, as well as their reported subcellular localization (24). Phylogenetic sequence analysis indicates that ACBD2/ECI2 represents a separate gene family from other related genes, such as mitochondrial ECH short-chain 1, peroxisomal ECH1, and ECI1, with the bootstrap support values over 50%, a

statistical approach to estimate resampling distribution (Supplemental Figure 1). Genome-wide analyses indeed supported this concept, indicating that the *Acbd2/Eci2* gene can be traced down to bacterial enoyl-CoA hydrolases, and its closest domain sequence is the ECH in mammalian testis-specific chromodomain Y-like proteins, instead of the ECH domain of ECI1. Even though there is such a divergence between the ECH domains from ACBD2/ECI2 and ECI1, previous mouse gene disruption studies proposed that these domains are functionally complementary (23, 24). Sequence alignment and 3-dimensional mapping of important residues between these 2 protein families showed the conserved functional residues in isomerase, but with a slight shift in the alignment that may reflect the preference of favorable substrates, such as long-chain fatty acids or medium-chain fatty acids within each subcellular niche (such as peroxisomes or mitochondria) (data not shown).

To identify the biological function of the *Acbd2/Eci2* gene relevant to our research focus on Leydig cell steroid biosynthesis, we used the Molecular Signatures Database (www.broadinstitute.org/gsea) and previously published Rat Genome 230 2.0 Array dataset probed with RNAs from rat Leydig cells isolated at different stages during development (GEO, GSE26703). We performed a GSEA and found that the fatty acid metabolism pathway was enriched during Leydig cell development, because it was present on the top ranking where the *Acbd2/Eci2*, *Eci1*, and *Echs1* genes are found within the same gene set; they were found with increased transcriptional expression during the developmental process from stem to adult Leydig cells (Supplemental Figure 2) (46). All 3 probes used for the *Acbd2/Eci2* gene in this microarray platform were up-regulated during this process, as well as under the hormone treatment of the MA-10 mouse tumor Leydig cells; this is a well-established cell model for studying the cellular and molecular mechanisms of steroidogenesis (47).

mRNA varieties encoding ACBD2/ECI2 protein isoform(s) via alternative splice site selection

To further investigate the different features of the 3 known mRNA transcript varieties of the *Acbd2/Eci2* gene that encode protein isoforms A and B, we adapted isoform-specific primers to amplify the corresponding portions of the gene. Surprisingly, in addition to the 3 known *Acbd2/Eci2* mRNA transcripts (A, B, and C), sequencing of PCR amplicons generated using each transcript's variety-specific primer showed the presence of 3 additional new transcript varieties in the MA-10 cells, which were designated as transcript varieties D, E, and F (Figure 2A). It seems that mRNA transcript varieties D, E, and F, as well as B and C, use the second ATG as the start codon for translation. Only the transcript variety A, encoding protein isoform A, utilizes the first ATG as a start codon, leading to an extended 5′-end sequence encoding the N-terminal mitochondrial targeting presequence (Figure 2B).

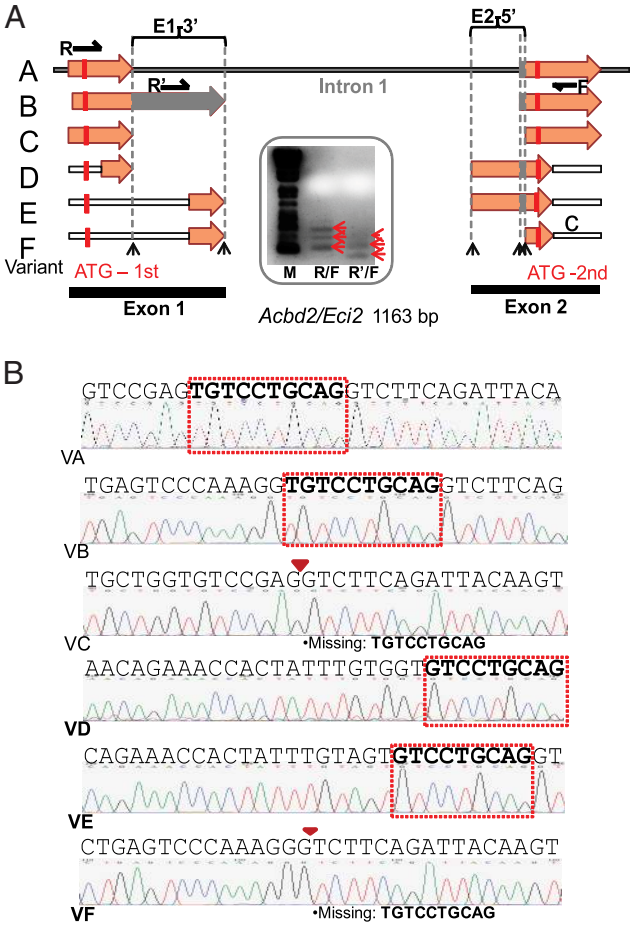

Figure 2. Identification of new varieties of *Acbd2/Eci2* mRNA sequences from gene-specific PCR, Sanger sequencing, and genomic mapping. A, Highlight of the genomic region from Exon 1 to Exon 2 of the *Acbd2/Eci2* gene, with 6 sequence varieties of *Acbd2/Eci2* transcripts from this genomic locus. Isoforms A, B, and C are the same sequence varieties as reported in GenBank (NM_001110331, NM_011868, and NR_073427, respectively), and 3 additional new sequence varieties found in MA-10 cells are presented as D, E, and F. First ATG and alternative second ATG (red bar), as well as alternative 3′-end of Exon 1 (E1–3′) and 5′-end of Exon 2 (E2–5′) splicing, are indicated with dotted lines. Gene-specific PCRs, either R/F or R′/F, for amplification of the portion between Exon 1 and Exon 2 are shown in the agarose gel photography (indel). M, 1 Kb plus DNA ladder (Invitrogen). Arrows indicate the PCR amplicons. B, Sequence chromatograms of *Acbd2/Eci2* mRNA varieties are shown as VA, VB, and VC, the 3 previously identified *Acbd2/Eci2* transcripts, which were further confirmed by sequence variety-specific PCRs; VD, VE, and VF represent the 3 additional, newly identified mRNA varieties. The red dotted rectangular square indicates the specific sequence, TGTCCTGCAG, that was missed from other sequence varieties. The red arrow indicates the site that misses 10 base sequence that is present in VA, VB, VD, and VE.

Transcriptional response to dbcAMP and immunofluorescent staining of endogenous peroxisomal ACBD2/ECI2 protein and its relationship to mitochondria

Given that *Acbd2/Eci2* has at least 3 known mRNA sequence varieties, we performed an isoform-specific melting curve analysis to distinguish which sequence variety is responsive to hormone treatment in MA-10 cells. The results obtained showed that the mRNA encoding the protein isoform A appears after 2 hours of treatment with the cAMP analog, dbcAMP, and after 10 hours without any treatment (Figure 3A). Because the slightest difference among the 3 *Acbd2/Eci2* mRNA varieties is only a 10 base deletion between 2 of the sequence varieties, which leads the first start codon to shift to the second available ATG, it results in the loss of the N-terminal presequence (Figure 2). The *Acbd2/Eci2* mRNA, with a few base sequence insertions, encodes the isoform A with a mitochondrial presequence. This phenomenon is apparently a result of alterative splice site selection (Figure 2).

To examine the subcellular distribution of the endogenous protein ACBD2/ECI2 proteins between mitochondria and peroxisomes in MA-10 cells, we used a goat anti-ACBD2/ECI2 polyclonal antibody in immunofluorescent staining to show that endogenous peroxisomal ACBD2/ECI2 was less colocalized with mitochondrial staining in MA-10 cells (Figure 3, B and C), but the mitochondrial colocalization was significantly increased in response to dbcAMP treatment (Figure 3, D and E). To validate the immunofluorescent staining of the endogenous proteins, we used gene-specific siRNA to knockdown the transcription of *Acbd2/Eci2* mRNA and used the control siRNA as negative control. The results ob-

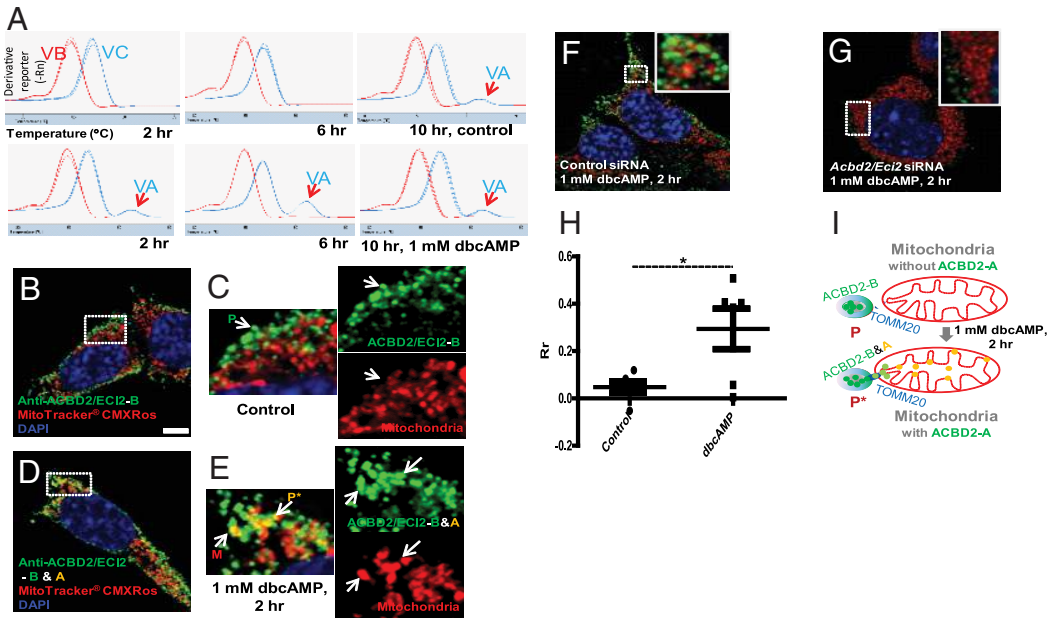

Figure 3. Emergence of *Acbd2/Eci2* variant A after dbcAMP treatment detected by melting curve analysis and its confirmation by immunofluorescence assay of endogenous ACBD2/ECI2 proteins. A, Melting curve profiles of each *Acbd2/Eci2* mRNA isoform from different pools of mRNAs in MA-10 Leydig tumor cells. mRNAs were collected at 2, 6, or 10 hours after treatment with 1mM dbcAMP. Fluorescence (derivative reporter, −Rn) on the y-axis was plotted against temperature (°C) on the x-axis. The higher melting temperature corresponds to the longer size and higher GC% of PCR products, which then determines the isoforms. VA, VB, and VC correspond to the *Acbd2/Eci2* mRNA varieties: A, B, and C, respectively. B and C, An immunocytofluorescence assay of ACBD2/ECI2 protein(s) in MA-10 cells before dbcAMP treatment. ACBD2/ECI2 proteins (green, by and large the isoform B) were detected in MA-10 cells by goat anti-PECI antibodies, which were imaged with secondary Alexa Fluor 488 donkey antigoat IgG (H+L) antibody. DAPI (blue) and MitoTracker CMXRos (red) were used as nuclear and mitochondria counterstaining, respectively. A highlighted region from the assay is shown in C, where the 2 separated channels (green and red) are shown on the right. D and E, An immunocytofluorescence assay of ACBD2/ECI2 protein(s) in MA-10 cells after dbcAMP treatment. ACBD2/ECI2 proteins (green, by and large the isoform B; yellow, the isoform A, the only form can be overlapped with mitochondrial staining) were detected in MA-10 cells by goat anti-PECI antibodies, which were imaged with secondary Alexa Fluor 488 donkey antigoat IgG (H+L) antibody. DAPI (blue) and MitoTracker CMXRos (red) were used as nuclear and mitochondria counterstaining, respectively. A highlighted region from the assay is shown in E, where the 2 separated channels (green and red) are shown on the right. Images were recorded using FV10-ASW 3.1 Viewer. P, peroxisomes; M, mitochondria. Scale bar, 5 μm. F and G, Knockdown of endogenous *Acbd2/Eci2* mRNA using control siRNAs (F) or *Acbd2/Eci2*-specific siRNAs (G) after dbcAMP treatment. Inset, The magnified area within the cell showing the colocalization of the anti-ACBD2/ECI2 protein (green) and MitoTracker CMXRos staining (red). The staining conditions are the same as shown in B–E. H, Correlation of immunocytofluorescent staining of ACBD2/ECI2 proteins in green with mitochondria in red. Rr values are close to 0.4 after the dbcAMP treatment, which is significantly higher than that of the control. Statistical analysis was performed using Student's *t* test; *, $P \leq .05$; n = 6. I, A diagram indicates the association of peroxisomal ACBD2/ECI2-isoforms B or B/A to mitochondria via peroxisomes (P) or P* before and after dbcAMP stimulation. TOMM20, presequence recognition by the OMM receptor subunit.

tained showed a dramatic reduction in the immunostaining of ACBD2/ECI2 proteins in contrast to that seen after treatment of the cells with control siRNA (Figure 3, F and G). Furthermore, we found that Rr analysis before and after the dbcAMP stimulation demonstrated the statistical significance of the colocalization between green/red channels (Figure 3H). These findings indicate that more ACBD2/ECI2 proteins were transported into the mitochondria of MA-10 cell in response to dbcAMP treatment; it is noteworthy that the only the ACBD2/ECI2 isoform A is capable of moving into mitochondria because of its N-terminal presequence (Figure 3I). This hypothesis was further validated using confocal laser-scanning microscopy for live-cell imaging and "In-cell co-IP" in 2 different Leydig cell lines MA-10 and mLTC1.

ACBD2/ECI2 protein targeting to peroxisomes and/or mitochondria

To determine whether and how ACBD2/ECI2 targets peroxisomes and/or mitochondria in MA-10 Leydig cells, we constructed 6 plasmids encoding ACBD2/ECI2-DsRed, ECI1-DsRed, ECI3-DsRed, DsRed-ACBD2/ECI2, DsRed-ECI1, and DsRed-ECI3, where the DsRed is a monomer red fluorescent protein designed against protein aggregation and 2 parallel control proteins, namely mitochondrial matrix protein ECI1 and the peroxisomal matrix protein ECI3 (Supplemental Table 1). Moreover, to avoid artifacts that may be generated when cotransfecting 2 plasmids simultaneously likely leads one protein affects another protein's subcellular targeting, we established a stable cell line that constitutively expresses mitochondrial roGFP, the Mito-H cell line, derived from MA-10 mouse Leydig cells (Supplemental Figure 3, A–E). Mito-H cells, generated by MA-10 cell transfection with roGFP, and cell sorting with the highest excitation at 474 nm, were then characterized as having high potential for steroid biosynthesis, likely due to its different redox subcellular environment (Supplemental Figure 3F).

To avoid the nonspecific signals in immunofluorescent staining of either the peroxisomal or mitochondrial matrix soluble proteins, we adapted live-cell imaging and confocal microscopy throughout this study that is less prone to be affected by experimental artifacts (48, 49). The typical plasmid constructs used in this study are shown in Figure 4A, where the protein under investigation was tagged with either a C- or N-terminal DsRed-monomer fluorescent protein, which apparently blocks its either N-terminal or C-terminal functional signal sequence, if there is any. We found that DsRed-ACBD2/ECI2 targets peroxisomes, using peroxisomal membrane protein marker AmCyan-PEX11β, which indicates that the C-terminal PST1 of ACBD2/ECI2, −Pro-Lys-Leu-COOH, functionally directs the protein into the peroxisomal matrix (Figure 4B), which is likely with the assistance of the PTS receptor PEX5 as previously reported (50, 51). In comparison with mitochondria, the DsRed-ACBD2/ECI2 containing peroxisomes are approaching the mitochondria and seem prone to penetrate the mitochondria (Figure 4C). In case of the ACBD2/ECI2 fused with a C-terminal DsRed tag, ACBD2/ECI2-DsRed remarkably targets to mitochondria by its predicted N-terminal mitochondrial targeting sequence (specifically, presequence) (Figure 4D), which is in assistance with the mitochondrial import receptor TOMM20 (52).

Similar subcellular localizations were observed with 2 control proteins: mitochondrial matrix protein ECI1 with an N-terminal presequence and peroxisomal matrix ECI3 with a C-terminal PST1 (Supplemental Figure 4, A–D), where ECI1-DsRed localized to mitochondria and ECI3-DsRed was in cytosol (Supplemental Figure 1, A and B). In contrast, DsRed-ECI1 with a blocked N-terminal presequence was in cytosol, whereas DsRed-ECI3 localized in peroxisomes because of its C-terminal PTS1-Ala-Lys-Leu-COOH tail (Supplemental Figure 4, C and D). These data suggest that the C-terminal tag blocked the access of the PTS1 receptor PEX5, whereas the N-terminal tag limited the access of its N-terminal presequence via TOMM20. Similar results were obtained using the mLTC1 mouse Leydig cell line where the DsRed-ACBD2/ECI2 (isoform B) was localized in peroxisomes and ACBD2/ECI2-DsRed (with blocked PTS1) was localized in mitochondria (Supplemental Figures 5 and 6).

Of the most interesting observation, the N-terminal presequence of DsRed-ACBD2/ECI2 is sufficiently potent to permit its translocation close to the mitochondria, even under the blockage effect induced by DsRed tag (Figure 5). These findings provide a tool to visualize the interactions of the organelles, such as the increased contacts or fusions after dbcAMP stimulation in MA-10 cells. To analyze the colocalization between DsRed-ACBD2/ECI2 containing peroxisomes and mitochondria, we transfected Mito-H cells with plasmid DsRed-ACBD2/ECI2. Confocal live-cell images were collected from the 2 groups with or without dbcAMP treatment, and the colocalized pixels between the green and red channels were highlighted using FV10-ASW software (version 3.1; Olympus). We found that dbcAMP treatment significantly increased the numbers of peroxisome-mitochondria contact sites or fusions, revealed by the colocalization pixels (Figure 5B), whereas the phenomenon was not observed with other 2 control proteins: DsRed-ECI1 and DsRed-ECI3 (Supplemental Figure 4, C and D). The quantification of green and red colocalized puncta that reflect the 2 organelles' contacts in the processed images

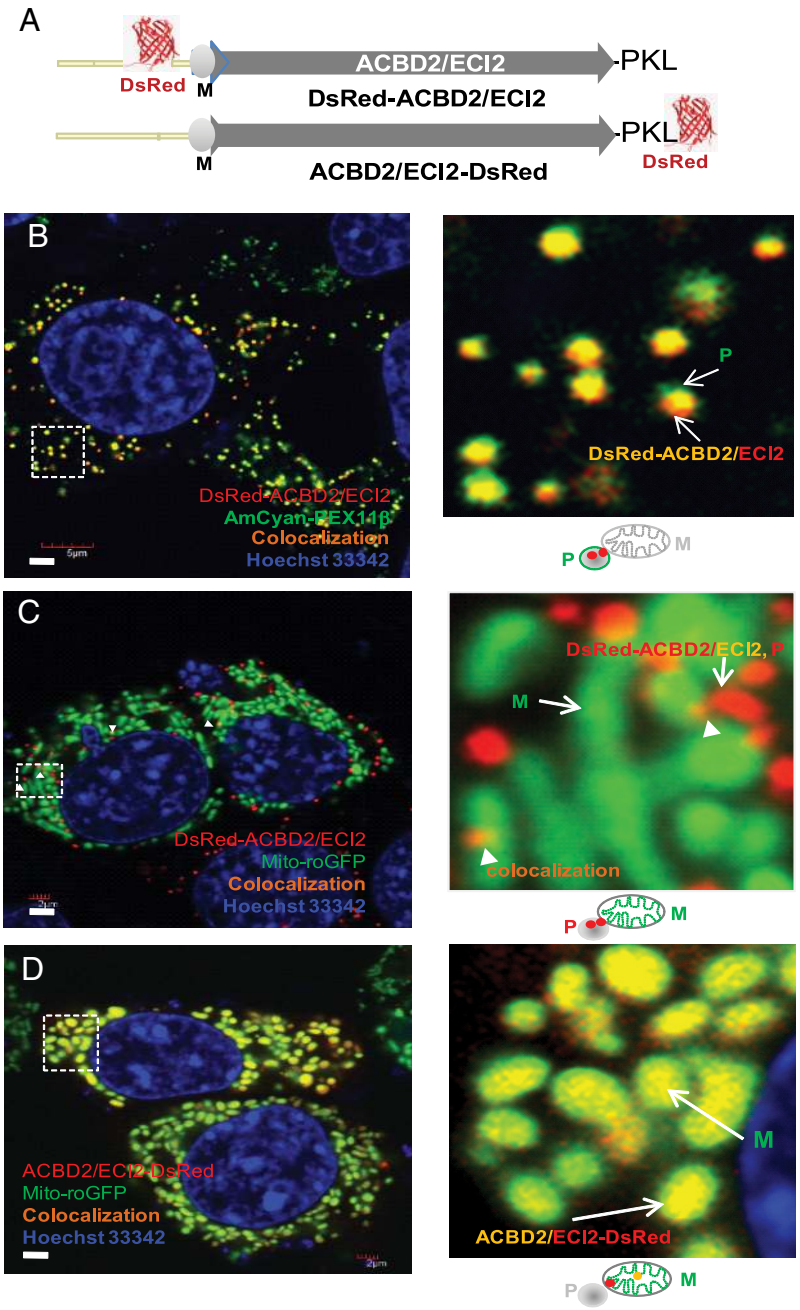

Figure 4. Subcellular targeting of ACBD2/ECI2 revealed by fluorescence live-cell imaging with confocal laser microscopy. A, Schematic diagrams of representative plasmid constructs DsRed-ACBD2/ECI2 and ACBD2/ECI2-DsRed used for live-cell imaging. The open reading frame of ACBD2/ECI2 was fused to either N terminus or C terminus of DsRed-monomer fluorescent protein (DsRed). M, mitochondrial presequence; −PKL, PTS1 signal sequence. B, Peroxisomal localization of DsRed-ACBD2/ECI2 fusion protein (red). AmCyan-PEX11β, peroxisomal membrane marker (green). PEX11β, a peroxisomal integral membrane protein 11β. Hoechst 33342, nuclei (blue). Scale bar, 2 μm. Magnified area is highlighted in right panel, where peroxisomal localization of DsRed-ACBD2/ECI2 is shown as yellow/red; and a diagram below indicates the peroxisomal location of ACBD2/ECI2. P, peroxisomes. M, mitochondria. C, Mitochondrial attachment of peroxisomal DsRed-ACBD2/ECI2 (red). Mito-roGFP was used as mitochondrial matrix marker in Mito-H cells (green). Hoechst 33342, nuclei (blue). Scale bar, 2 μm. Magnified region is shown in the right panel, and a diagram indicates the mitochondrial attachment of DsRed-ACBD2/ECI2. Colocalization between red and green, yellow. D, Mitochondrial localization of ACBD2/ECI2-DsRed fusion protein (Red). Mito-roGFP, mitochondrial matrix marker (green). Hoechst 33342, nuclei (blue). Scale bar, 2 μm. Magnification of the overlap between red/green channels is shown in the right panel, and a diagram indicates the mitochondrial localization of ACBD2/ECI2-DsRed.

was performed using ImageJ software (V. 1.47j; NIH) (Figure 5, C and D). To corroborate and validate our observation, we adapted Duolink, the In-cell co-IP assay to assess the interaction between the peroxisomal ACBD2/ECI2 (note that only the isoform A has potential mitochondrial targeting) and the OMM marker protein TOMM20. The positive PLA signals revealed the interaction between ACBD2 and TOMM20, suggesting the dynamic interplay between peroxisomes and mitochondria. These data were further validated using a different Leydig cell line, mLTC1, as shown in Supplemental Figure 7. The increased peroxisome-mitochondria interactions after dbcAMP stimulation may reflect their coordinated function in the metabolism of fatty acids, removal of reactive oxygen species/superoxide radicals, and steroid biosynthesis (1, 53) (Figure 5, E–H).

A peroxisome-like structure, the "peroxisomal cargo" (P*), carrying PTS1 proteins while approaching mitochondria

To mimic the endogenous domain structure of ACBD2/ECI2, we constructed a new plasmid, mito-DsRed-ACBD2/ECI2, that produces a protein with a structure similar to its native protein, where the N-terminal presequence of ACBD2/ECI2 was moved from its native position to be in front of the DsRed tag, and the C-terminal PTS1 remains untouched (Figure 6A). After transfection with this plasmid in Mito-H cells, we observed interestingly that the protein showed dual targeting to both peroxisomes and mitochondria, where the colocalization with mito-roGFP (mitochondrial matrix protein marker) indicates the mitochondrial localization of ACBD2/ECI2, the colocalization with AmCyan-PMP70 (peroxisomal membrane protein marker) indicates the perox-

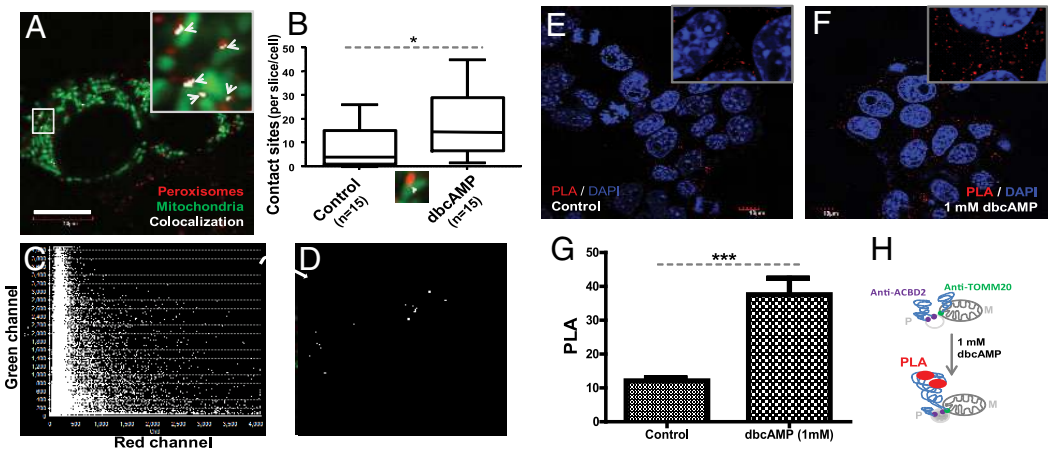

Figure 5. Quantitative colocalization analysis of contact sites or "fusion" between peroxisomes and mitochondria in response to dbcAMP revealed by DsRed-ACBD2/ECI2. A, A representative image of the cells showing the colocalization (white) of peroxisomal DsRed-ACBD2/ECI2 (red) and mito-roGFP (green), as highlighted in insert. Arrows indicate the contact sites or fusions between the peroxisomes and mitochondria. Scale bar, 10 μm. B, Box-and-whiskers plots of the numbers of ACBD2/ECI2-mediated contact sites between peroxisomes and mitochondria before and after dbcAMP treatment. The high-power image below the graph highlights an example of the quantified contact sites. Statistical analysis was performed using a Mann-Whitney test (*, $P < .05$; n = 15 cells on single optical section). C and D, A scatterplot of red and green pixel intensities of the image as shown in A. The scatterplot is split into 4 areas, quadrants (C). The upper-right quadrant represents pixels with high intensity levels in both green and red, which can be used to calculate colocalization pixels from 2 channels: DsRed-ACBD2/ECI2 and Mito-roGFP as shown in D and A. E and F, Colocalization between endogenous ACBD2/ECI2 (peroxisomes) and TOMM20 (mitochondria) visualized by the PLA Duolink-In-cell co-IP (red) in cultures without (E) and at present of 1mM dbcAMP for 2 hours (F). Inset, The magnified area to show the red blobs as the PLA signals. G, Bar graphs of the quantification of colocalized ACBD2/ECI2 and TOMM20 puncta or contact sites revealed before and after 1mM dbcAMP treatment. Mean ± SD; ***, Student's *t* test, $P < .001$; n = 291 (control) and n = 220 (1mM dbcAMP). H, A diagram of PLA between ACBD2/ECI2 and TOMM20. ACBD2/ECI2-A appeared in response to dbcAMP treatment as the N-terminal presequence that binds to the OMM receptor TOMM20. Anti-ACBD2 and anti-TOMM20mantibodis are indicated. PLA, red dots; P, peroxisomes; M, mitochondria.

isomal localization, and apparently some proteins present in-between the mitochondria and the peroxisomes with no colocalization with PMP70 that was estimated from a total fluorescence intensity using mitochondrial and peroxisomal staining for the ROI (region-of-interest) calculation (Figure 6, B–D). These data strongly suggest that in MA-10 cells the native ACBD2/ECI2 protein not only localizes in the peroxisomes (Figure 6B), but it also localizes in the mitochondria (Figure 6C); in addition, a prominent amount of protein was found between the peroxisomes and mitochondria and it seems that it is in an ongoing "tug of war" between these 2 organelles viewed as the mito-DsRed-ACBD2/ECI2 protein which may involve the 2 matrix protein complex transporters: PEX5 and TOMM20 (see below), where the strong solid red fluorescence indicates the protein localization outside the mitochondria (labeled as P*), the weak cristae-like fluorescence indicates its localization inside the mitochondria (labeled as M), and the asymmetric localization of mito-DsRed-ACBD2/ECI2 (red) with AmCyan-mPMP70 (green) (labeled as P) indicates that mito-DsRed-ACBD2/ECI2 protein with the peroxisomes still associated with mitochondrial targeting complex proteins (see below) (Figure 6C). The percentage of total fluorescence intensity per cell is 48% in mitochondria, determined using roGFP labeling, and 23% in peroxisomes, determined using mPMP70 labeling, and the rest 29% found in the position approaching mitochondria (P*) (Figure 6D), which was not seen with the overexpression of the fluorescent tag alone and with the 2 other control fluorescently tagged proteins (Supplemental Figure 4; see below). Similar results were obtained using mLTC1 Leydig cells, where we used a 3 colors system to visualize protein and organelle localization: mito-DsRed-ACBD2/ECI2 (isoform A) seen as red, peroxisomes (peroxisomal matrix protein AcGFP-pero) seen as green, and mitochondria (mitochondrial matrix protein mito-BFP) seen as blue (Supplemental Figure 8).

To further investigate whether and how the peroxisomal ACBD2/ECI2 is associated with mitochondria, we did subcellular fractionation of the MA-10 cell whole-cell lysates and immunoblot analysis (Figure 6E). Endogenous ACBD2/ECI2 protein is strongly associated with the mitochondrial fraction but weakly associated with peroxisomal fraction, where the COX IV as mitochondrial marker, SCPX as peroxisomal marker, and the GAPDH as loading control. The ACBD2/ECI2-mitochondrial association was confirmed by the colocalization data between the voltage-dependent anion-selective channel protein 1 (VDAC1) and ACBD2/ECI2 obtained with confocal immunofluorescence imaging analysis (Figure 6F). The dominant costaining of the VDAC1 and ACBD2/ECI2 was seen as mitochondria shown as the large punctate structures, whereas some of the observed small punctate

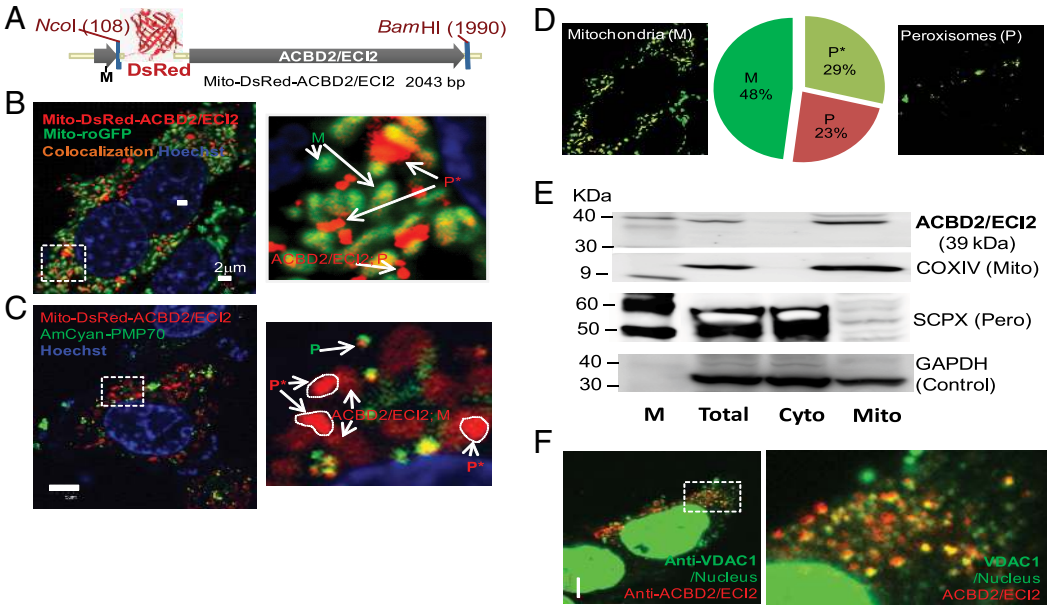

Figure 6. Reconstruction of native ACBD2/ECI2 protein isoform A. A, A diagram of the plasmid construct of mito-DsRed-ACBD2/ECI2, a mimic of the native ACBD2/ECI2 protein structure, where both N and C termini are free. Two restriction enzymes used in the cloning are shown as *Nco*I and *Bam*HI. M, presequence; DsRed, DsRed-monomer fluorescent protein. B, Confocal laser microscopy live-cell imaging of mito-DsRed-ACBD2/ECI2 protein in Mito-H cells. Mito-DsRed-ACBD2/ECI2, red; Mito-roGFP, green indicating mitochondria; Hoechst (blue), nuclei. Higher magnification of a partial image is shown in the right panel. P, peroxisomes; M, mitochondria. Scale bar, 2 μm. C, Confocal laser microscopy live-cell image of mito-DsRed-ACBD2/ECI2 protein (red) and peroxisomal membrane marker: AmCyan-mPMP70 (green), in Mito-H cells. Hoechst (blue), nuclei. Scale bar, 5 μm. D, A pie chart depicting the representative quantitative analysis of the subcellular localization of mito-DsRed-ACBD2/ECI2 protein in a cell. The fluorescence intensity of the protein in mitochondria (M) was determined to be 48% based on mito-roGFP labeling, 23% in peroxisomes (P) based on mPMP70 labeling and 29% found between these 2 organelles (P*) determined as the ratio to the total fluorescence intensity per cell. Left panel, An image extracted from B to show the mitochondrial mito-DsRed-ACBD2/ECI2. Right panel, An image extracted from C to show the peroxisomal Mito-DsRed-ACBD2/ECI2. E, Immunoblot analysis of the endogenous ACBD2/ECI2 in the subcellular fractions of MA-10 cell lysates. COX IV is used as an inner mitochondrial membrane marker protein (Mito); SCPX is used as peroxisomal marker (Pero); and GAPDH as a whole-cell lysate-loading control. M, protein marker as indicated in kDa; Total, whole-cell lysate; Cyto, cytosol fractions; Mito, mitochondrial-enriched fraction. F, Double immunofluorescent staining of endogenous ACBD2/ECI2 in MA-10 cells (in red) and VDAC1 (an OMM marker; painted in green). Nucleus was also counterstained with DAPI (painted in green). The magnified partial staining is shown at the right panel. Scale bar, 5 μm.

dots may represent other subcellular compartments, likely involving ER/mitochondria-associated membranes (54).

To characterize the interorganellar distribution of ACBD2/ECI2 between peroxisomes and mitochondria, colocalization studies of mito-DsRed-ACBD2/ECI2 with AmCyan-mPEX11β (peroxisomal membrane protein marker) were performed in MA-10 cells. The results obtained showed that the peroxisome-like structure lost the peroxisomal integral membrane protein, PEX11β (Figure 7A). However, it is colocalized partially with the AmCyan-pero (peroxisomal matrix protein marker), indicating that the PTS1-targeting proteins can still be loaded into the P* (Figure 7B). This phenomenon was not observed using in the peroxisomal and mitochondrial dual-targeting control protein, mito-DsRed-pero, where the PEX11β as peroxisomal membrane protein marker and mito-roGFP as mitochondrial matrix protein marker (Figure 7, C and D). We believe that peroxisomes loaded with ACBD2/ECI2 change their structure/composition when approaching the mitochondria, as the P*, in the interorganellar communication. It is likely that this finding may represent an asymmetric distribution of ACBD2/ECI2 in the peroxisomes, which likely be caused by the competitive binding of peroxisomal receptor PEX5, of mitochondrial receptor TOMM20, and/or other unknown components involving in the ACBD2/ECI2 protein.

The association of ACBD2/ECI2 protein with the peroxisomal import receptor PEX5, the mitochondrial import receptor subunit TOMM20 and the PTS1 proteins are illustrated as a tug of war as shown in Figure 8A, where the PEX5 binds the PTS1 signal of the peroxisomal matrix proteins to assist the PTS1-protein peroxisomal import, and TOMM20 assists the presequence-containing mitochondrial matrix proteins into the mitochondria (55, 56). In both cases, the ACBD2/ECI2 protein involves these 2 organelles' matrix protein import receptor complexes. Ectopic expression of TOMM20 leads to mitochondrial localization of the mito-DsRed-ACBD2/ECI2,

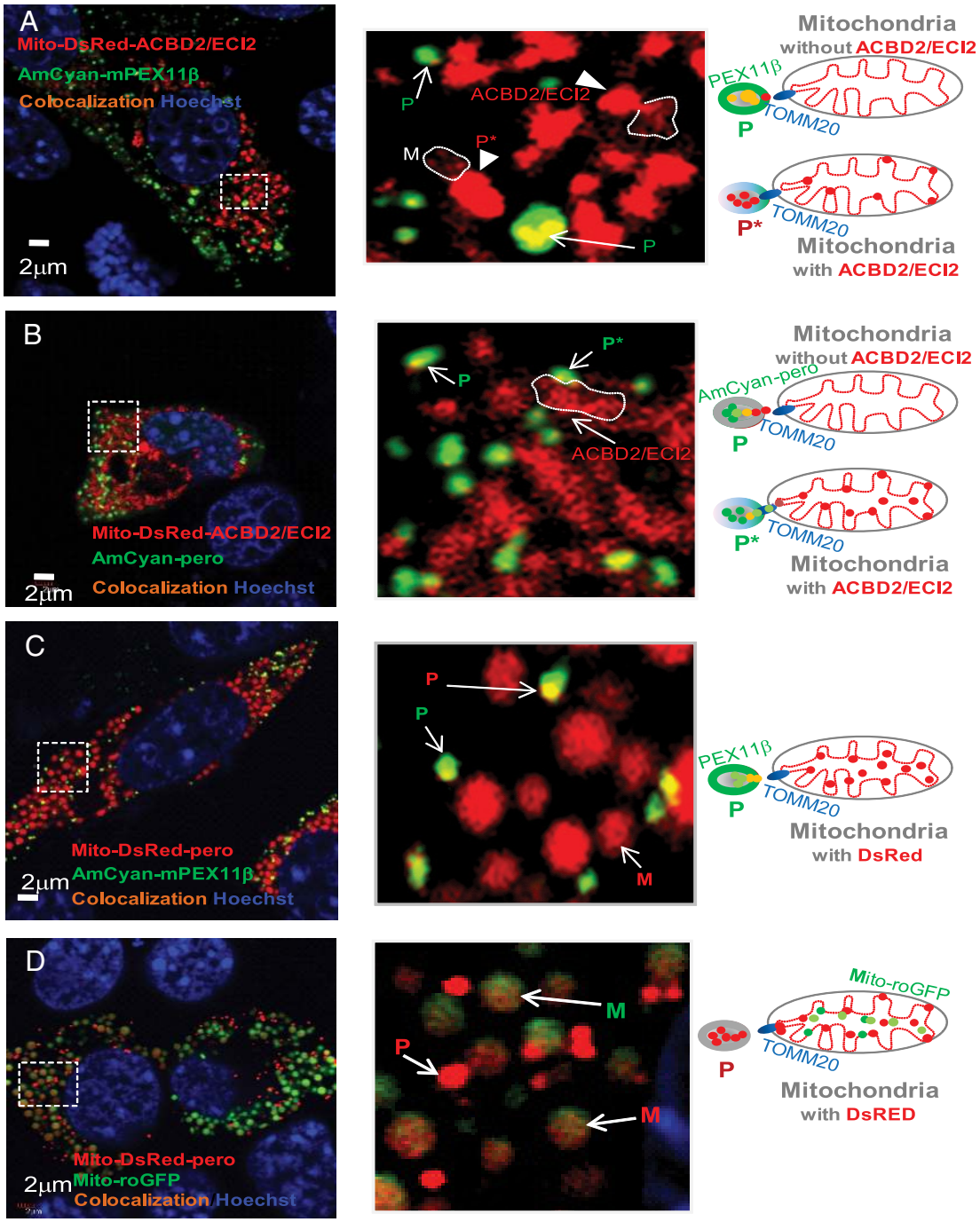

Figure 7. Mito-DsRed-ACBD2/ECI2 mediated peroxisome-like structure, the P*. A, Colocalization analysis of mito-DsRed-ACBD2/ECI2 (red) with the peroxisomal integral membrane protein AmCyan-mPEX11β (green). Hoechst (blue), nuclei. A magnified staining is shown in middle panel. P, peroxisomes; P*, white arrow; M, mitochondria (dotted line). Scale bar, 2 μm. A diagram in the right panel shows the relationship between peroxisomes and mitochondria revealed by ACBD2/ECI2. Isolated peroxisomes (green) show that ACBD2/ECI2 (red) is inside the PEX11β or on one side; the peroxisomes (red) associated with mitochondria are connected as P* via TOMM20. B, Colocalization analysis of mito-DsRed-ACBD2/ECI2 (red) with peroxisomal matrix protein AmCyan-pero (green). Hoechst (blue), nuclei. A magnified staining is shown in middle panel. P*, connected to mitochondria; M, dotted line, indicated by ACBD/ECI2. Scale bar, 2 μm. A diagram in the right panel shows the relationship between peroxisomes and mitochondria revealed by ACBD2/ECI2. Isolated peroxisomes (green) show that ACBD2/ECI2 (red) is on one side of the organelle; the peroxisomes (green) associated with mitochondria are connected as P* via TOMM20. C, Colocalization analysis of a dual-targeting control protein, mito-DsRed-pero (red), with AmCyan-mPEX11β (green). Hoechst (blue), nuclei. A magnified staining is shown in middle panel. P, green/yellow; M, red. Scale bar, 2 μm. A diagram in the right panel shows that peroxisomes contain peroxisomal membrane protein PEX11β (green) and matrix mito-DsRed-pero (red) located on one side of the organelle, whereas mitochondria contains only matrix mito-DsRed-pero (red). D, Colocalization analysis of mito-DsRed-pero (red) with mitochondrial matrix protein Mito-roGFP (green). Hoechst (blue), nuclei. An enlarged highlight is shown in middle panel. Scale bar, 2 μm. A diagram in the right panel indicates that peroxisomes contain only matrix mito-DsRed-pero (red), whereas mitochondria contain both matrix mito-DsRed-pero (red) and matrix Mito-roGFP (green).

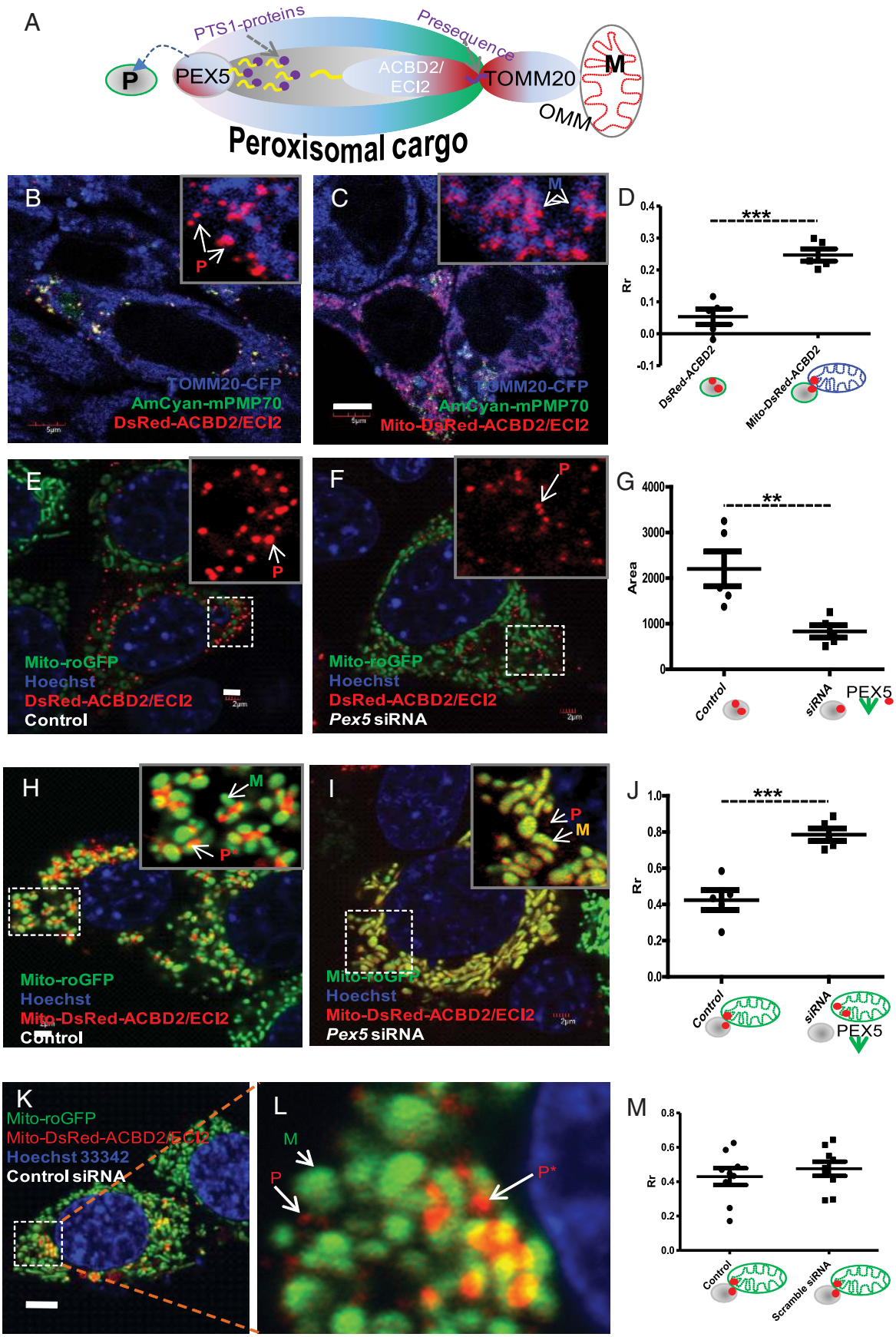

Figure 8. Formation of the P* involves PEX5 and TOMM20 from 2 subcellular matrix protein import receptor complexes, respectively. A, A diagrammatic structure of a putative P*. PEX5, PTS receptor; PTS1-proteins, PTS1 containing proteins; Presequence, mitochondrial targeting

but not to the DsRed-ACBD2/ECI2, where it shows a significant difference ($P < .001$) in Rr (Figure 8, B–D). Knockdown of PEX5 by siRNAs resulted in decreased peroxisomal import, revealed by small peroxisomes with significant less fluorescence intensity (Figure 8, E–G), while leading to redistribution of mito-DsRed-ACBD2/ECI2 from peroxisomes and P* to mitochondria (Figure 8, H–J). However, the control siRNA had no significant effect on the redistribution of the dual-targeting protein (Figure 8, K and M). It is of great interest that the 0.4 Rr value obtained from the expression of artificial mito-DsRed-ACBD2/ECI2 is similar to that observed with immunofluorescent staining of the endogenous peroxisomal ACBD2/ECI2 (Figure 3H). Although the antibody used recognizes all ACBD2/ECI2 isoforms, only the ACBD2/ECI2 isoform A has the potential to be relocated to or connected with mitochondria. Its biological significance could have a wider implication, because the ACBD2/ECI2 isoform A was shown to be widely distributed in tissues/organs other than those making steroids (Supplemental Figure 9). Therefore, we believe that the mito-DsRed-ACBD2/ECI2 could be used as a tool to monitor the native protein behavior before and after the dbcAMP treatment and its association with peroxisome-mitochondria interactions in steroid biosynthesis in steroidogenic cells and various metabolic pathways in nonsteroidogenic cells.

Figure 8. (Continued). sequence; TOMM20, mitochondrial import receptor subunit; P, peroxisomes; M, mitochondria. B–D, Ectopic express of TOMM20 (blue) has no effect on peroxisomal localization of DsRed-ACBD2/ECI2 (red) (B) but leads to mitochondrial localization of mitoDsRed-ACBD2/ECI2 (red) (C), with counterstaining of peroxisomes using 70-kDa peroxisomal membrane protein-AmCyan-mPMP70 (green). Scale bar, 5 μm. Rr from C is far from zero and is significantly different from that in B, indicating the mitochondrial import of the mito-DsRed-ACBD2/ECI2 protein (D). A diagram showing the peroxisomal localization of DsRed-ACBD2/ECI2 and peroxisomal and mitochondrial dual localizations of mito-DsRed-ACBD2/ECI2 is indicated below each scatter plot. Statistical analysis was performed using Student's *t* test; ***, $P \leq .001$; n = 5. E–G, Knockdown of PEX5 using *Pex5*-specific siRNAs leads to less accumulation of DsRed-ACBD2/ECI2 (peroxisomal matrix protein). The area of peroxisomes before and after PEX5 knockdown was measured and the PEX5 knockdown cells have significant low intensity and/or numbers. Scale bar, 2 μm. A diagram showing the peroxisomal localization of DsRed-ACBD2/ECI2 and its decreased peroxisomal localizations under the deficiency of PEX5 is indicated below each scatter plot. Statistical analysis was performed using Student's *t* test; ** $P \leq .01$; n = 5. H–J, Knockdown of PEX5 using specific siRNAs validated from E–G leads to the prevailing accumulation of the mito-DsRed-ACBD2/ECI2 in mitochondria. The Rr values are close to 1 and significantly different from that of control cells where P* can be formed, indicating the mitochondrial localization of the mito-DsRed-ACBD2/ECI2 protein. Scale bar, 2 μm. A diagram showing the peroxisomal and mitochondrial dual localizations of mito-DsRed-ACBD2/ECI2 and loss of peroxisomal location under the deficiency of PEX5 is indicated below each scatter plot. Statistical analysis was performed using Student's *t* test; ***, $P \leq .001$; n = 5. K–M, Using control siRNAs leads to no change of the subcellular distribution of mito-DsRed-ACBD2/ECI2 protein, which is similar to the pattern from control cells in H. Scale bar, 5 μm. A diagram showing no change of the peroxisomal and mitochondrial dual localizations of mito-DsRed-ACBD2/ECI2 using control siRNA is indicated below each scatter plot. Statistical analysis of the Rr values was performed using Student's *t* test; $P = .48$; n = 9.

ACBD2/ECI2 mediated peroxisome-mitochondria contacts lead to increased steroid formation

To further assess the biological significance of the ACBD2/ECI2-mediated close contact between peroxisomes and mitochondria, we constructed a series of plasmids that encode the protein without the ACBP domain (No-Acbp), and 3 control proteins such as the peroxisomal and mitochondrial dual-targeting matrix protein, mito-DsRed-pero (DsRedc), peroxisomal DsRed-ACBD2/ECI2 (Pero), and mitochondrial ACBD2/ECI2-DsRed (Mito), in addition to the full protein mito-DsRed-ACBD2/ECI2 (isoform A) (Figure 9A). We then transfected each of them into Mito-H cells and nontransfected cells were used as control; finally we measured the progesterone formed in the media. Both ACBP and ECH domains were found to be required for ACBD2/ECI2 function in basal steroid biosynthesis, in addition to their role in peroxisomes, mitochondria contacts (Figure 9B), and also the protein without the ACBP domain failed to potentiate by 1.45-fold the dbcAMP maximally induced progesterone formation in contrast to the mito-DsRed-ACBD2/ECI2 which resembles the endogenous protein (Figure 9C). However, the expression of control protein DsRed either in peroxisomes or in mitochondria or in both organelles had no significant effect on steroid production (Figure 9, B and C).

Alternative splicing regulation controls the subcellular localization of ACBD2-ECI2

Because only 1 of the 6 sequence varieties (at least) of the *Acbd2/Eci2* was identified to encode a protein with potential dual targeting of both peroxisomes and mitochondria, and given that the rest encode a protein that targets only peroxisomes, it is obvious that the phenomenon is initially controlled by a mechanism of active alternative splicing regulation as previously reported in fungi (57). The ACBD2/ECI2 isoform A targets both peroxisomes and mitochondria as illustrated with a diagram and magnified confocal images in Figure 10. The mRNA encoding this protein is controlled at the transcriptional level via an alternative splicing site selection. This alternative splicing selection leads to the subcellular distribution of the protein(s) on dual targeting of the peroxisomes and mitochondria via a P*, or at the peroxisomes, or at the mitochondria alone under certain circumstances (Figure 10A). The dual-targeting feature of the ACBD2/ECI2-A from unfolded nascent protein to mature protein

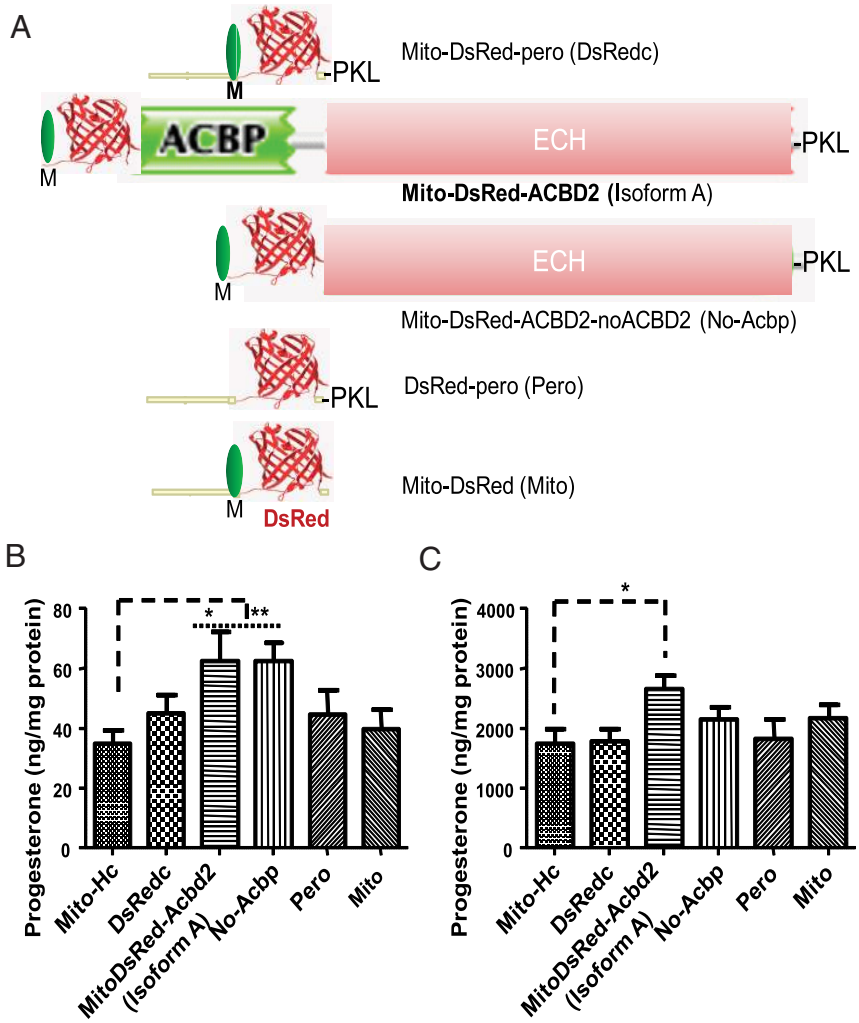

Figure 9. Increased steroid production under the ectopic expression of native ACBD2/ECI2 protein isoforms A. A, Diagrams of 5 plasmid constructs were used in this study. Each plasmid name is shown with an abbreviation in the brackets and also in the bar graphs (B and C). DsRed, DsRed-monomer fluorescent protein; M, mitochondrial presequence; −PKL, the PTS1 peptide sequence. B and C, Measurement of progesterone release from the Mito-H cells at the basal level (B) and 2 hours after dbcAMP treatment (C). Bar graphs represent the progesterone measurement (ng/mL protein) in Mito-H cells transfected with different plasmids: mitoHc, control; DsRedc, mito-DsRed-pero plasmid as vector control; Mito-DsRed-Acbd2, mito-DsRed-ACBD2/ECI2 plasmid; No-Acbp, mito-DsRed-ACBD2/ECI2 without ACBP domain; Pero, DsRed with a C-terminal peroxisomal targeting; Mito, DsRed with an N-terminal mitochondrial targeting sequence. Data are shown as the mean ± SD from 4 independent experiments performed in triplicate. Statistical analysis was performed using Student's *t* tests; *, $P < .05$; **, $P < .01$; n = 4.

packed as P*, which involves the 2 organelle matrix protein import receptor complexes PEX5 and TOMM20, plays a role in MA-10 steroidogenesis via its contact between the peroxisomes and mitochondria (Figure 10B).

Discussion

Functional complementarity between ACBD2/ECI2 and ECI1 via the subcellular redistribution of ACBD2/ECI2 isoform A

Current knowledge about the cellular localization and function of the ACBD2/ECI2 protein has been confusing and incomplete due to the lack of precise information about this protein, hampering further exploration into its biological significance. The *Acbd2/Eci2* gene encodes 2 protein isoforms: A and B, and there is no anti-ACBD2/ECI2 isoform-specific antibody available to distinguish these 2 isoforms. In addition, immunostaining of endogenous soluble matrix proteins would likely misidentify the subcellular localization of the ACBD2/ECI2 isoforms due to the technical limitations of immunolabeling (49). However, these limitations could be overcome by live-cell imaging where no diffusion through the membrane permeabilization occurs (49).

Recent reports on the functional redundancy in the oxidation of unsaturated fatty acids between the *Acbd2/Eci2* and *Eci1*, generated from knockdown and/or knockout mice, could be properly interpreted now by the characterization of protein isoform identity, domain structure, sequence similarity, subcellular compartments, as well as by the ACBD/ECI2-mediated interorganelle interplay. Although the ECH domain in ECI1 is evolutionarily distantly related to the one in ACBD2/ECI2, it may share the same and/or similar cellular functions within different subcellular compartments. It is noteworthy that all the ECH domains belong to the low-similarity isomerase/hydratase or crotonase superfamily (58, 59). Among the various isoforms of ACBD2/ECI2, the isoform A under certain conditions (for example, cAMP stimulation) can be formed via alternative splicing, and then moved/transported into the mitochondria in a form of P* via its presequence (60) and its PTS1 tripeptide. Therefore, the role of each protein may be determined by specific subcellular segregation; the ECI1 is a mitochondrial-targeting protein, both ECI3 and ACBD2/ECI2 isoform B are peroxisomal-targeting proteins, and ACBD2/ECI2 isoform A is either a peroxisomal- or mitochondrial-targeting protein, leading to the formation of a peroxisomal "cargo" consisting of the 2 peroxisomal and mitochondrial matrix transport complexes in tethering between these 2 organelles.

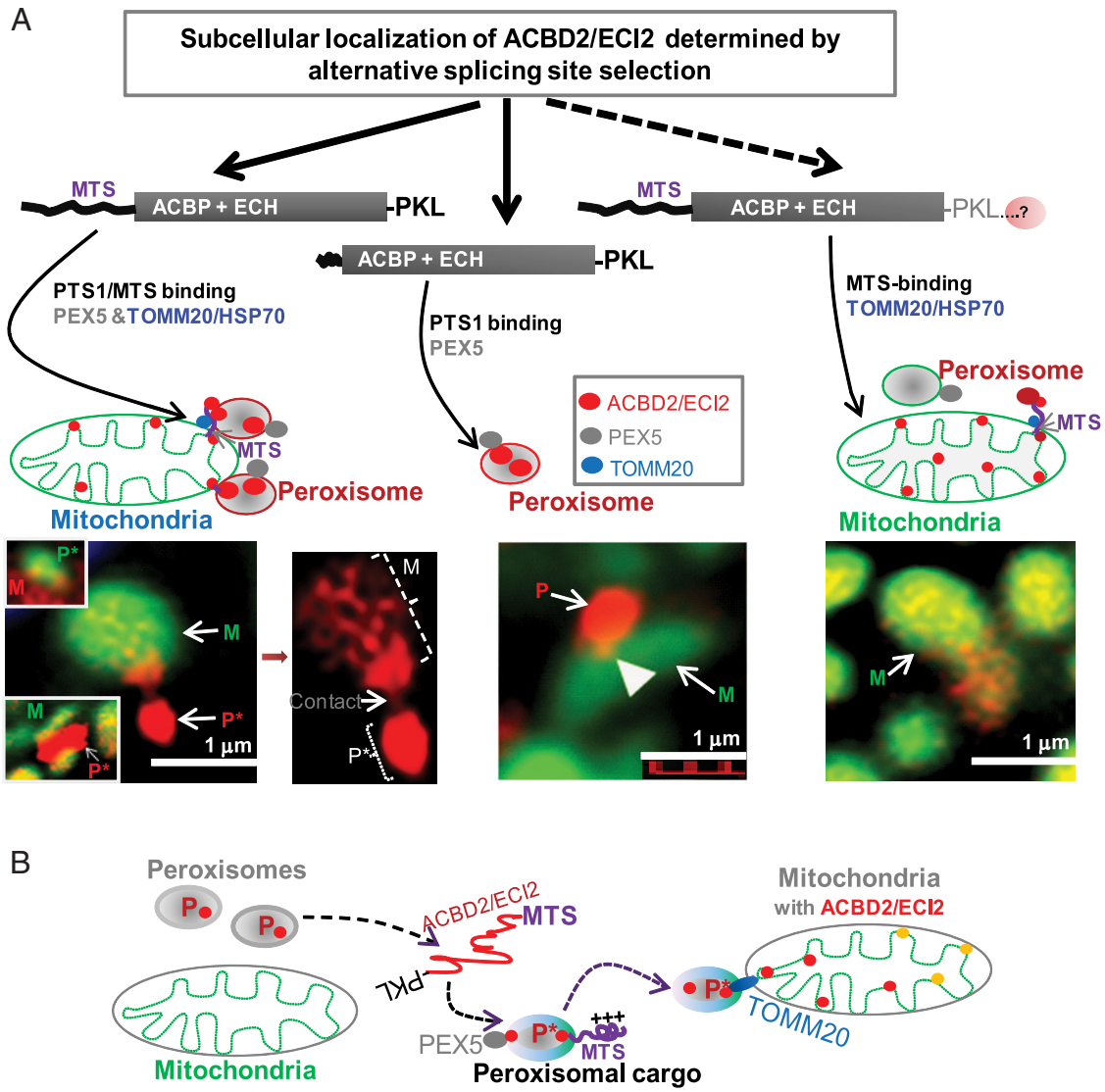

Figure 10. Subcellular targeting of ACBD2/ECI2 determined by alternative splicing receptor site selection. A, A summary diagram of the protein subcellular targeting via the alternative autosplicing site selection, as well as a representative image to show P*, peroxisomes (contact site), and mitochondria viewed by fluorescent ACBD2/ECI fusion protein (red). Three different mature mRNAs lead to different protein transport pathways: an ACBD2/ECI2-mediated dual-targeting pathway to both the mitochondria and peroxisomes at the same time via a competitive binding mechanism between PEX5 and TMM20/HSP70, resulting in close contact between the 2 organelles left panel); folded peroxisomal matrix protein(s) targeting to peroxisomes via PTS1 receptor PEX5 (middle panel); and unfolded mitochondrial matrix protein(s) targeting the mitochondria via the mitochondrial import receptor complex, TOMM20/HSP70 (right panel). The dotted line in the diagram indicates an artificial transcript fused with a fluorescence tag (a pink oval) at its 3′-end of −PKL. The corresponding representative highly magnified confocal image supporting each proposed model is shown underneath each panel. Detailed distribution of the dual targeting protein between the peroxisome-like structure and mitochondria is highlighted in a single red channel. Scale bar, 1 μm. M, mitochondria; P, peroxisomes; MTS, mitochondrial targeting signal; −PKL, the potential PTS1 sequence in ACBD2/ECI2 protein; HSP70, 70-kDa chaperone heat shock protein; PEX5, PTS1 receptor. B, A schematic diagram of the P* mediated by ACBD2/ECI2 via PEX5 (gray dot) and TOMM20 (blue) in approaching the mitochondria. Red spots within peroxisomes, P*, or mitochondria represent the mitochondrial and peroxisomal dual-targeting protein, ACBD2/ECI2. MTS, MTS with positively charged amino acids (+++); −PKL, the potential PTS1 sequence of ACBD2/ECI2.

The finding that each one of these proteins has a distinct subcellular organelle localization is in agreement with the phenotype observed in the knockdown of *Acbd2/Eci2* in *Eci1*-deficient fibroblasts and under the presence of a third paralogous *Eci3* gene in the mouse genome (24). Thus, functional redundancy between ECI1 and ACBD2/ECI2 isoform A in mitochondria, and the same holds true for ECI3 and ACBD2/ECI2 isoform B in peroxisomes, will set up the basis upon which to interpret previous genetic studies in mice, and to guide further experimental design in animal models.

Functional relationship of the *Acbd2/Eci2* gene to steroid biosynthesis and lipid metabolism during Leydig cell development

During Leydig cell development, the transcription expression profiles of steroidogenic genes are dramatically

up-regulated, as we expected from several previous reports about the role of Leydig cells in steroidogenesis (46, 61–63). In addition, fatty acid metabolism-related gene expression, including *Acbd2/Eci2* and *Eci1*, is also up-regulated, which is related to the β-oxidation of fatty acids during Leydig cell development. Our observation is consistent with the disappearance of lipid droplets in morphology from the conversion of immature to adult Leydig cells (62, 64). Considering that one of the main sources of cholesterol used for steroid biosynthesis stems from esterified cholesterol where a fatty acid must be metabolized accordingly during this process, we suppose that ACBD2/ECI2 plays an import role during this process (31). We have confirmed that ACBD2/ECI2 isoform A has a subcellular response to the human chorionic gonadotropin's second messenger cAMP, which is tested here using its analog dbcAMP. This phenomenon is actually reflected in the increased functional interplay between the peroxisomes and mitochondria after cAMP stimulation.

Peroxisome-mitochondria contacts in response to dbcAMP treatment and it significance in steroid biosynthesis

Several reports showed the functional relationship between peroxisomes and mitochondria in mammalian cells, but few are on their close contact yet (1, 11, 65). This interorganelle association between peroxisomes and mitochondria was previously observed in the electron micrographs of rat Leydig cells treated with gonadotropin LH, where 3–4 organelle fusions were shown in each cell (66). Additionally, few examples of morphological connection between peroxisomes and mitochondria have been presented in low eukaryotic organisms, such as fission unicellular yeasts and green algae (67, 68). Regardless of its morphology, an unknown mechanism underlying this phenomenon remains. So far, we only know a 1-way connection from the mitochondria to the peroxisomes via mitochondria-derived vesicles (11, 69–71). However, during the β-oxidation of very long-chain fatty acids and other substrate metabolism, 2-way communication between the peroxisomes to the mitochondria is essential because the final product of peroxisomal β-oxidation is octanoyl-coenzyme A, which is a preferred substrate of mitochondrial β-oxidation enzymes, such as ECI1, for the further production of acetyl-CoA in the citric acid cycle (72). Aging-related reduced production of testosterone in Leydig cells is likely due to changes in intracellular processing and metabolism of cholesteryl esters as well as cholesterol trafficking into mitochondria and availability for steroidogenesis (73, 74). Considering that the amount of the steroidogenic substrate cholesterol available is rate-limiting, but not the enzymes CYP11A1 and 3β-hydroxysteroid dehydrogenase responsible for its metabolism of cholesterol to pregnenolone and then progesterone, the increased progesterone could reflect the amount of cholesterol transported into mitochondria and thus available for steroid formation (29, 41). Therefore, ACBD2/ECI2 likely plays a role and/or assists in supplying cholesterol used for steroid biosynthesis. Additional accumulated evidence so far has shown the close functional contact/relationship between peroxisomes and mitochondria, and even the physical contact between these 2 organelles has been proposed diagrammatically in a recent review. Nevertheless, those are mostly derived from the studies in unicellular yeasts (65). Considering that the yeast ortholog of ACBD2/ECI2 has no N-terminal presequence, our report here provides a valuable tool in reviewing the physical contact between peroxisomes and mitochondria, implying that it plays an essential role in the striking close relationship between peroxisomes and mitochondria in mammals.

The tug of war between peroxisomes and mitochondria involves a peroxisome-like structure, the P*

In addition to the fact that both the ACBP- and ECH-domains of ACBD2/ECI2 are required for basal and dbcAMP-induced steroid biosynthesis via a close contact between the peroxisomes and the mitochondria, the native domain structure of ACBD2/ECI2 is required for tethering of the P* to mitochondria, which differs from the previously described juxtaposed elongated peroxisome-like structures, which mediates the effect of PEX11s in membrane tabulation (75). Both PEX11β and PMP70 are not present in the membrane of the P* that may represent a different form of peroxisomes (35). The live-cell imaging of fluorescently tagged proteins could reflect the endogenous proteins revealed by subcellular compartmentation of native ACBD2/ECI2 from immunofluorescence, even though the antibody cannot exclusively recognize the isoform A. In addition, both Rr values in the dbcAMP stimulation and in the ectopic expression of the ACBD2/ECI2 protein, indicating that the endogenous protein isoform A is inducible and plays a role in steroid biosynthesis. Overall, these findings indicate that the P* mediated by ACBD2/ECI2 plays an essential role in establishing 2-way communication between the peroxisomes and the mitochondria for lipid metabolism and steroid synthesis.

Alternative splicing regulation controls subcellular localization

Alternative splicing is a primary mechanism for controlling gene expression in a tissue-specific manner, and it

even expands the proteome (25, 76). The specific mRNA species encoding ACBD2/ECI2 isoform A is responsive to the dbcAMP treatment of the MA-10 Leydig cells. Only a few examples of alternative splicing have been linked to function (77–79). Although the N-terminal sequence of a protein provides a variety of organelle-targeting signals, no study has ever shown that alternative splicing determines protein targeting via the manipulation of organelle-specific targeting sequences (80). Given that the only one sequence variety encoding a full mitochondrial targeting presequence in the ACBD2/ECI2 isoform A is a result of "proper" alternative splicing, the rest of the transcripts could be regarded as either over or less autospliced products with 10-bp deletion and/or the embracing of more intron sequences, which leads to the reading frame shifting at their 5′-ends. Such a minor disparity among the transcript varieties could challenge the current approaches that are used to study its function in detail. The knockdown of the endogenous *Acbd2/Eci2* gene seems to be an attractive approach when studying its biological function of the protein(s), as performed previously (24), but it is a challenge to perform this sort of study to target one specific isoform with only a 10-bp difference from the rest. However, the effect of gene knockdown can be examined by its unique mitochondrial localization of ACBD2/ECI2 isoform A.

Our report suggests the existence of a molecular switch at the transcriptional level that extends beyond the dual-targeting of ACBD2/ECI2 in either the peroxisomes, mitochondria, or both organelles. Several examples of dual-targeting proteins by a similar mechanism have been reported previously (81–88), but none of them is related to peroxisomes/mitochondria. Moreover, previous large-scale peroxisomal proteomic studies have provided more likely peroxisomal and mitochondrial dual-targeting proteins (Supplemental Table 2) (89), but whether any other protein behaves in the same way as ACBD2/ECI2 remains be determined.

Conclusions

Alternative splicing of *Acbd2/Eci2* pre-mRNA creates an N-terminal mitochondrial presequence to the peroxisomal ACBD/ECI2 protein and then leads a tug of war between peroxisomes and mitochondria. Visualization of the mito-ACBD2/ECI2 subcellular localization could serve as a valuable tool for studying the live interorganelle tethering between peroxisomes and mitochondria, and its function in cholesterol transport into mitochondria and steroidogenesis. The accordant relationship between the interorganelle connection and cellular function is associated not only with both N-terminal mitochondrial presequence and C-terminal PTS sequence of ACBD2/ECI2, but also with 2 core domains: ECH and ACBP, of the protein. The ACBD2/ECI2 structural and functional model in Leydig cell steroidogenesis as reported here opens up a new avenue to address the dynamics of peroxisomes and their relationship to the biological contributions of mitochondria.

Acknowledgments

We thank Dr Mario Ascoli (University of Iowa, Iowa City, IA) for supplying the MA-10 cell line.

Address all correspondence and requests for reprints to: Vassilios Papadopoulos, The Research Institute of the McGill University Health Centre, Glen Site, 1001 Boulevard Décarie, Block E, Room E013152, Montréal, QC, Canada H4A 3J1. E-mail: vassilios.papadopoulos@mcgill.ca.

Author contributions: J.F. and V.P. designed the experiments and wrote the manuscript draft; J.F. conducted the confocal microscopy live-cell imaging and molecular cloning; X.L. was involved in the construction and characterization of several plasmids; L.I. performed biochemical studies; and J.F., M.C., and V.P. edited and finalized the manuscript.

This work was supported by the Canadian Institutes of Health Research Grant MOP-102647 and the Canada Research Chair in Biochemical Pharmacology (V.P.). The Research Institute of McGill University Health Centre was supported by a center grant from Le Fonds de Recherche du Québec-Santé.

Disclosure Summary: The authors have nothing to disclose.

References

1. **Schrader M, Yoon Y.** Mitochondria and peroxisomes: are the 'big brother' and the 'little sister' closer than assumed? *Bioessays*. 2007; 29:1105–1114.
2. **Smallridge R.** Membrane trafficking: mitochondria-peroxisome connection. *Nat Rev Mol Cell Bio*. 2008;9:186–187.
3. **Smith JJ, Aitchison JD.** Peroxisomes take shape. *Nat Rev Mol Cell Bio*. 2013;14:803–817.
4. **Elbaz Y, Schuldiner M.** Staying in touch: the molecular era of organelle contact sites. *Trends Biochem Sci*. 2011;36:616–623.
5. **Friedman JR, Lackner LL, West M, DiBenedetto JR, Nunnari J, Voeltz GK.** ER tubules mark sites of mitochondrial division. *Science*. 2011;334:358–362.
6. **Rowland AA, Voeltz GK.** Endoplasmic reticulum-mitochondria contacts: function of the junction. *Nat Rev Mol Cell Bio*. 2012;13: 607–625.
7. **Rambold AS, Lippincott-Schwartz J.** Cell biology. SevERing mitochondria. *Science*. 2011;334:186–187.
8. **Hoepfner D, Schildknegt D, Braakman I, Philippsen P, Tabak HF.** Contribution of the endoplasmic reticulum to peroxisome formation. *Cell*. 2006;122:85–95.
9. **Titorenko VI, Mullen RT.** Peroxisome biogenesis: the peroxisomal endomembrane system and the role of the ER. *J Cell Biol*. 2006; 174:11–17.
10. **van der Zand A, Gent J, Braakman I, Tabak HF.** Biochemically

distinct vesicles from the endoplasmic reticulum fuse to form peroxisomes. *Cell*. 2012;149:397–409.
11. **Neuspiel M, Schauss AC, Braschi E, et al.** Cargo-selected transport from the mitochondria to peroxisomes is mediated by vesicular carriers. *Curr Biol*. 2008;18:102–108.
12. **Schumann U, Subramani S.** Special delivery from mitochondria to peroxisomes. *Trends Cell Biol*. 2008;18:253–256.
13. **Nordgren M, Fransen M.** Peroxisomal metabolism and oxidative stress. *Biochimie*. 2014;98:56–62.
14. **Hua R, Kim PK.** Multiple paths to peroxisomes: mechanism of peroxisome maintenance in mammals. *Biochim Biophys Acta*. 2016;1863:881–891.
15. **Camões F, Islinger M, Guimaraes SC, et al.** New insights into the peroxisomal protein inventory: acyl-CoA oxidases and -dehydrogenases are an ancient feature of peroxisomes. *Biochim Biophys Acta*. 2015;1853:111–125.
16. **Reddy JK, Mannaerts GP.** Peroxisomal lipid metabolism. *Annu Rev Nutr*. 1994;14:343–370.
17. **Faust PL, Kovacs WJ.** Cholesterol biosynthesis and ER stress in peroxisome deficiency. *Biochimie*. 2014;98:75–85.
18. **Kovacs WJ, Olivier LM, Krisans SK.** Central role of peroxisomes in isoprenoid biosynthesis. *Prog Lipid Res*. 2002;41:369–391.
19. **Liu J, Li H, Papadopoulos V.** PAP7, a PBR/PKA-RIα-associated protein: a new element in the relay of the hormonal induction of steroidogenesis. *J Steroid Biochem Mol Biol*. 2003;85:275–283.
20. **Fan J, Liu J, Culty M, Papadopoulos V.** Acyl-coenzyme A binding domain containing 3 (ACBD3; PAP7; GCP60): an emerging signaling molecule. *Prog Lipid Res*. 2010;49:218–234.
21. **Geisbrecht BV, Zhang D, Schulz H, Gould SJ.** Characterization of PECI, a novel monofunctional Δ3, Δ2-enoyl-CoA isomerase of mammalian peroxisomes. *J Biol Chem*. 1999;274:21797–21803.
22. **Zhang D, Yu W, Geisbrecht BV, Gould SJ, Sprecher H, Schulz H.** Functional characterization of Δ3,Δ2-enoyl-CoA isomerases from rat liver. *J Biol Chem*. 2002;277:9127–9132.
23. **Janssen U, Stoffel W.** Disruption of mitochondrial β-oxidation of unsaturated fatty acids in the Δ^3, Δ^2-trans-enoyl-CoA isomerase-deficient mouse. *J Biol Chem*. 2002;277:19579–19584.
24. **van Weeghel M, te Brinke H, van Lenthe H, et al.** Functional redundancy of mitochondrial enoyl-CoA isomerases in the oxidation of unsaturated fatty acids. *FASEB J*. 2012;26:4316–4326.
25. **Wang ET, Sandberg R, Luo S, et al.** Alternative isoform regulation in human tissue transcriptomes. *Nature*. 2008;456:470–476.
26. **Baumgart E, Schad A, Völkl A, Fahimi HD.** Detection of mRNAs encoding peroxisomal proteins by non-radioactive in situ hybridization with digoxigenin-labelled cRNAs. *Histochem Cell Biol*. 1997;108:371–379.
27. **Rone MB, Fan J, Papadopoulos V.** Cholesterol transport in steroid biosynthesis: role of protein-protein interactions and implications in disease states. *BBA-Mol Cell Biol L*. 2009;1791:646–658.
28. **Papadopoulos V, Baraldi M, Guilarte TR, et al.** Translocator protein (18kDa): new nomenclature for the peripheral-type benzodiazepine receptor based on its structure and molecular function. *Trends Pharmacol Sci*. 2006;27:402–409.
29. **Papadopoulos V, Miller WL.** Role of mitochondria in steroidogenesis. *Best Pract Res Cl En*. 2012;26:771–790.
30. **Rone MB, Midzak AS, Issop L, et al.** Identification of a dynamic mitochondrial protein complex driving cholesterol import, trafficking, and metabolism to steroid hormones. *Mol Endocrinol*. 2012;26:1868–1882.
31. **Hou JW, Collins DC, Schleicher RL.** Sources of cholesterol for testosterone biosynthesis in murine Leydig cells. *Endocrinology*. 1990;127:2047–2055.
32. **Lüers GH, Schad A, Fahimi HD, Völkl A, Seitz J.** Expression of peroxisomal proteins provides clear evidence for the presence of peroxisomes in the male germ cell line GC1spg. *Cytogenet Genome Res*. 2003;103:360–365.
33. **Lüers GH, Thiele S, Schad A, Völkl A, Yokota S, Seitz J.** Peroxisomes are present in murine spermatogonia and disappear during the course of spermatogenesis. *Histochem Cell Biol*. 2006;125:693–703.
34. **Huyghe S, Schmalbruch H, De Gendt K, et al.** Peroxisomal multifunctional protein 2 is essential for lipid homeostasis in Sertoli cells and male fertility in mice. *Endocrinology*. 2006;147:2228–2236.
35. **Schrader M, King SJ, Stroh TA, Schroer TA.** Real time imaging reveals a peroxisomal reticulum in living cells. *J Cell Sci*. 2000;113:3663–3671.
36. **Thompson JD, Gibson T, Higgins DG.** Multiple sequence alignment using ClustalW and ClustalX. *Curr Protoc Bioinformatics*. 2002;Unit:2.3.
37. **Saitou N, Nei M.** The neighbor-joining method: a new method for reconstructing phylogenetic trees. *Mol Biol Evol*. 1987;4:406–425.
38. **Tamura K, Peterson D, Peterson N, Stecher G, Nei M, Kumar S.** MEGA5: molecular evolutionary genetics analysis using maximum likelihood, evolutionary distance, and maximum parsimony methods. *Mol Biol Evol*. 2011;28:2731–2739.
39. **Irizarry RA, Hobbs B, Collin F, et al.** Exploration, normalization, and summaries of high density oligonucleotide array probe level data. *Biostatistics*. 2003;4:249–264.
40. **Subramanian A, Tamayo P, Mootha VK, et al.** Gene set enrichment analysis: a knowledge-based approach for interpreting genome-wide expression profiles. *Proc Natl Acad Sci USA*. 2005;102:15545–15550.
41. **Ascoli M.** Characterization of several clonal lines of cultured Leydig tumor cells: gonadotropin receptors and steroidogenic responses. *Endocrinology*. 1981;108:88–95.
42. **Hanson GT, Aggeler R, Oglesbee D, et al.** Investigating mitochondrial redox potential with redox-sensitive green fluorescent protein indicators. *J Biol Chem*. 2004;279:13044–13053.
43. **Fredriksson S, Gullberg M, Jarvius J, et al.** Protein detection using proximity-dependent DNA ligation assays. *Nat Biotechnol*. 2002;20:473–477.
44. **Fan J, Papadopoulos V.** Transcriptional regulation of translocator protein (*Tspo*) via a SINE B2-mediated natural antisense transcript in MA-10 Leydig cells. *Biol Reprod*. 2012;86:1–15.
45. **Papadopoulos V, Amri H, Li H, Boujrad N, Vidic B, Garnier M.** Targeted disruption of the peripheral-type benzodiazepine receptor gene inhibits steroidogenesis in the R2C Leydig tumor cell line. *J Biol Chem*. 1997;272:32129–32135.
46. **Stanley EL, Johnston DS, Fan J, et al.** Stem Leydig cell differentiation: gene expression during development of the adult rat population of Leydig cells. *Biol Reprod*. 2011;85:1161–1166.
47. **Fan J, Traore K, Li W, et al.** Molecular mechanisms mediating the effect of mono-(2-ethylhexyl) phthalate on hormone-stimulated steroidogenesis in MA-10 mouse tumor Leydig cells. *Endocrinology*. 2010;151:3348–3362.
48. **Melan MA, Sluder G.** Redistribution and differential extraction of soluble proteins in permeabilized cultured cells. Implications for immunofluorescence microscopy. *J Cell Sci*. 1992;101:731–743.
49. **Schnell U, Dijk F, Sjollema KA, Giepmans BN.** Immunolabeling artifacts and the need for live-cell imaging. *Nat Methods*. 2012;9:152–158.
50. **Otera H, Setoguchi K, Hamasaki M, Kumashiro T, Shimizu N, Fujiki Y.** Peroxisomal targeting signal receptor Pex5p interacts with cargoes and import machinery components in a spatiotemporally differentiated manner: conserved Pex5p WXXXF/Y motifs are critical for matrix protein import. *Mol Biol Cell*. 2002;22:1639–1655.
51. **Miyata N, Fujiki Y.** Shuttling mechanism of peroxisome targeting signal type 1 receptor Pex5: ATP-independent import and ATP-dependent export. *Mol Biol Cell*. 2005;25:10822–10832.
52. **Abe Y, Shodai T, Muto T, et al.** Structural basis of presequence recognition by the mitochondrial protein import receptor Tom20. *Cell*. 2000;100:551–560.
53. **Weinhofer I, Kunze M, Forss-Petter S, Berger J.** Involvement of human peroxisomes in biosynthesis and signaling of steroid and

peptide hormones. In: *Peroxisomes and Their Key Role in Cellular Signaling and Metabolism*. New York, NY: Springer; 2013;101–110; Editors: Luis A. del Río, Depto. Bioquímica, Biología Celular y, Estación Experimental del Zaidín, CSIC.
54. **Sabirov RZ, Merzlyak PG.** Plasmalemmal VDAC controversies and maxi-anion channel puzzle. *BBA-Biomembranes*. 2012;1818:1570–1580.
55. **Gatto GJ, Geisbrecht BV, Gould SJ, Berg JM.** Peroxisomal targeting signal-1 recognition by the TPR domains of human PEX5. *Nat Struct Mol Biol*. 2000;7:1091–1095.
56. **Saitoh T, Igura M, Obita T, et al.** Tom20 recognizes mitochondrial presequences through dynamic equilibrium among multiple bound states. *EMBO J*. 2007;26:4777–4787.
57. **Freitag J, Ast J, Bölker M.** Cryptic peroxisomal targeting via alternative splicing and stop codon read-through in fungi. *Nature*. 2012;485:522–525.
58. **Hubbard PA, Yu W, Schulz H, Kim JJ.** Domain swapping in the low-similarity isomerase/hydratase superfamily: the crystal structure of rat mitochondrial Δ^3, Δ^2-enoyl-CoA isomerase. *Protein Sci*. 2005;14:1545–1555.
59. **Holden HM, Benning MM, Haller T, Gerlt JA.** The crotonase superfamily: divergently related enzymes that catalyze different reactions involving acyl coenzyme a thioesters. *Accounts Chem Res*. 2001;34:145–157.
60. **Li NC, Fan J, Papadopoulos V.** Sterol carrier protein-2, a nonspecific lipid-transfer protein, in intracellular cholesterol trafficking in testicular Leydig cells. *PLoS One*. 2016; 11:e0149728.
61. **Haider SG.** Leydig cell steroidogenesis: unmasking the functional importance of mitochondria. *Endocrinology*. 2007;148:2581–2582.
62. **Chen H, Stanley E, Jin S, Zirkin BR.** Stem Leydig cells: from fetal to aged animals. *Birth Defects Res Part C Embryo Today*. 2010;90:272–283.
63. **Ge RS, Dong Q, Sottas CM, Papadopoulos V, Zirkin BR, Hardy MP.** In search of rat stem Leydig cells: identification, isolation, and lineage-specific development. *Proc Natl Acad Sci USA*. 2006;103:2719–2724.
64. **Mendis-Handagama SM, Ariyaratne HB.** Differentiation of the adult Leydig cell population in the postnatal testis. *Biol Reprod*. 2001;65:660–671.
65. **Mohanty A, McBride HM.** Emerging roles of mitochondria in the evolution, biogenesis, and function of peroxisomes. *Front Physiol*. 2013;4:268.
66. **Mendis-Handagama SM.** Peroxisomes and intracellular cholesterol trafficking in adult rat Leydig cells following luteinizing hormone stimulation. *Tissue Cell*. 2000;32:102–106.
67. **Jourdain I, Sontam D, Johnson C, Dillies C, Hyams JS.** Dynamin-dependent biogenesis, cell cycle regulation and mitochondrial association of peroxisomes in fission yeast. *Traffic*. 2008;9:353–365.
68. **Miyagishima Sy, Itoh R, Toda K, Kuroiwa H, Nishimura M, Kuroiwa T.** Microbody proliferation and segregation cycle in the single-microbody alga *Cyanidioschyzon merolae*. *Planta*. 1999;208:326–336.
69. **Andrade-Navarro MA, Sanchez-Pulido L, McBride HM.** Mitochondrial vesicles: an ancient process providing new links to peroxisomes. *Curr Opin Cell Biol*. 2009;21:560–567.
70. **Braschi E, Goyon V, Zunino R, Mohanty A, Xu L, McBride HM.** Vps35 mediates vesicle transport between the mitochondria and peroxisomes. *Curr Biol*. 2010;20:1310–1315.
71. **Soubannier V, Rippstein P, Kaufman BA, Shoubridge EA, McBride HM.** Reconstitution of mitochondria derived vesicle formation demonstrates selective enrichment of oxidized cargo. *PLoS One*. 2012;7:e52830.
72. **Eaton S, Bartlett K, Pourfarzam M.** Mammalian mitochondrial β-oxidation. *Biochem J*. 1996;320:345–357.
73. **Liao C, Reaven E, Azhar S.** Age-related decline in the steroidogenic capacity of isolated rat Leydig cells: a defect in cholesterol mobilization and processing. *J Steroid Biochem Mol Biol*. 1993;46:39–47.
74. **Midzak AS, Chen H, Papadopoulos V, Zirkin BR.** Leydig cell aging and the mechanisms of reduced testosterone synthesis. *Mol Cell Endocrinol*. 2009;299:23–31.
75. **Koch J, Pranjic K, Huber A, et al.** PEX11 family members are membrane elongation factors that coordinate peroxisome proliferation and maintenance. *J Cell Sci*. 2010;123:3389–3400.
76. **Maniatis T, Tasic B.** Alternative pre-mRNA splicing and proteome expansion in metazoans. *Nature*. 2002;418:236–243.
77. **Nilsen TW, Graveley BR.** Expansion of the eukaryotic proteome by alternative splicing. *Nature*. 2010;463:457–463.
78. **Gabut M, Samavarchi-Tehrani P, Wang X, et al.** An alternative splicing switch regulates embryonic stem cell pluripotency and reprogramming. *Cell*. 2011;147:132–146.
79. **Nijholt I, Farchi N, Kye M, et al.** Stress-induced alternative splicing of acetylcholinesterase results in enhanced fear memory and long-term potentiation. *Mol Psychiatr*. 2003;9:174–183.
80. **Iwashita S, Tsuchida M, Tsukuda M, et al.** Multiple organelle-targeting signals in the N-terminal portion of peroxisomal membrane protein PMP70. *J Biochem*. 2010;147:581–590.
81. **Ashibe B, Hirai T, Higashi K, Sekimizu K, Motojima K.** Dual subcellular localization in the endoplasmic reticulum and peroxisomes and a vital role in protecting against oxidative stress of fatty aldehyde dehydrogenase are achieved by alternative splicing. *J Biol Chem*. 2007;282:20763–20773.
82. **Huang LJ, Wang L, Ma Y, et al.** NH_2-terminal targeting motifs direct dual specificity A-kinase-anchoring protein 1 (D-AKAP1) to either mitochondria or endoplasmic reticulum. *J Cell Biol*. 1999;145:951–959.
83. **Trotter KW, Fraser ID, Scott GK, Stutts MJ, Scott JD, Milgram SL.** Alternative splicing regulates the subcellular localization of A-kinase anchoring protein 18 isoforms. *J Cell Biol*. 1999;147:1481–1492.
84. **Tabuchi M, Tanaka N, Nishida-Kitayama J, Ohno H, Kishi F.** Alternative splicing regulates the subcellular localization of divalent metal transporter 1 isoforms. *Mol Biol Cell*. 2002;13:4371–4387.
85. **Ganesh S, Suzuki T, Yamakawa K.** Alternative splicing modulates subcellular localization of laforin. *Biochem Bioph Res Co*. 2002;291:1134–1137.
86. **Péterfy M, Phan J, Reue K.** Alternatively spliced lipin isoforms exhibit distinct expression pattern, subcellular localization, and role in adipogenesis. *J Biol Chem*. 2005;280:32883–32889.
87. **Clements JA, Mercer FC, Paterno GD, Gillespie LL.** Differential splicing alters subcellular localization of the α but not β isoform of the MIER1 transcriptional regulator in breast cancer cells. *PLoS One*. 2012;7:e32499.
88. **Zhang SC, MacDonald KA, Baguma-Nibasheka M, Geldenhuys L, Casson AG, Murphy PR.** Alternative splicing and differential subcellular localization of the rat FGF antisense gene product. *BMC Mol Biol*. 2008;9:10.
89. **Wiese S, Gronemeyer T, Ofman R, et al.** Proteomics characterization of mouse kidney peroxisomes by tandem mass spectrometry and protein correlation profiling. *Mol Cell Proteomics*. 2007;6:2045–2057.